Electrochemical Preparation of Platinum Isocyanide Clusters Containing Chelating Diphosphines. An Unprecedented Trinuclear Platinum Complex Involving a Coordinatively Unsaturated Metal Center, [{Pt(diphosphine)(isocyanide)}$_2$Pt](PF$_6$)$_2$[1a]

Tomoaki Tanase, Hirokazu Ukaji, Yasuko Kudo, Masahiro Ohno, Kimiko Kobayashi,[1b] and Yasuhiro Yamamoto*

Department of Chemistry, Faculty of Science, Toho University, Miyama 2-2-1, Funabashi-shi, Chiba 274, Japan

Received November 2, 1993®

A controlled-potential electrolysis was performed on mononuclear platinum(II) complexes containing aromatic isocyanide (RNC) and diphosphine (diphos) ligands, [Pt(diphos)(RNC)$_2$](PF$_6$)$_2$ (diphos = *cis*-1,2-bis(diphenylphosphino)ethene (dppen) (**1**), 1,2-bis(diphenylphosphino)ethane (dppe) (**2**), 1,3-bis(diphenylphosphino)propane (dppp) (**3**), 1,4-bis(diphenylphosphino)butane (dppb) (**4**), and 1,2-bis(di-*tert*-butylphosphino)ethane (dtbpe) (**5**); R = 2,6-dimethylphenyl or 2,4,6-trimethylphenyl), which were derived from the reaction of PtCl$_2$(COD) with diphos, RNC, and NH$_4$PF$_6$. Electrolyses of complexes **1**–**4** at a mercury-pool electrode consumed 1 F mol^{-1} in acetonitrile at −1.45 to −1.5 V (vs Cp$_2$Fe/Cp$_2$Fe$^+$), which gave dinuclear platinum(I) complexes, [Pt$_4$(diphos)$_2$(RNC)$_2$](PF$_6$)$_2$ (diphos = dppen (**6**), dppe (**7**), dppp (**8**), and dppb (**9**)). The compounds were characterized by IR, electronic, and ^{1}H and ^{31}P{^{1}H} NMR spectroscopy and X-ray crystallographic and EXAFS (extended X-ray absorption fine structure) analyses. Complex **8b** (R = 2,4,6-Me$_3$C$_6$H$_2$, diphos = dppp) crystallizes in the monoclinic system, space group $P2_1/c$, with a = 14.941(4) Å, b = 19.268(6) Å, c = 26.002(9) Å, β = 101.23(2)°, and Z = 4 (R = 0.059 and R_w = 0.051 for 5704 independent reflections with $I > 3\sigma(I)$). Complex **8b** consists of two platinum atoms, each coordinated by one isocyanide, one diphosphine as a chelating ligand, and the neighboring platinum atom in a square planar array. The length of the Pt–Pt bond is 2.653(1) Å. EXAFS analyses showed that the Pt–Pt bond lengths of **6**–**9** fall within the narrow range of 2.625–2.653 Å. Electrolyses of **1**, **3**, and **5** consumed 1.5 F mol^{-1} at ca. −1.8 V, which gave trinuclear platinum complexes, [{Pt(diphos)(RNC)}$_2$Pt](PF$_6$)$_2$ (diphos = dppen (**13**), dppp (**14**), and dtbpe (**15**)). Complex **13a** (R = 2,6-Me$_2$C$_6$H$_3$) crystallizes in the monoclinic system, space group $P2/n$, with a = 14.956(4) Å, b = 12.395(2) Å, c = 22.923(7) Å, β = 104.35(2)°, and Z = 2 (R = 0.048 and R_w = 0.046 for 2872 independent reflections with $I > 3\sigma(I)$); complex **14a** (R = 2,6-Me$_2$C$_6$H$_3$) crystallizes in the monoclinic system, space group $P2_1$, with a = 15.491(3) Å, b = 22.575(5) Å, c = 10.883(3) Å, β = 107.48(2)°, and Z = 2 (R = 0.056 and R_w = 0.038 for 3156 independent reflections with $I > 3\sigma(I)$); and complex **15a** (R = 2,6-Me$_2$C$_6$H$_3$) crystallizes in the monoclinic system, space group $C2/c$, with a = 19.489(6) Å, b = 15.284(5) Å, c = 25.804(6) Å, β = 116.34(2)°, and Z = 4 (R = 0.045 and R_w = 0.033 for 2904 independent reflections with $I > 3\sigma(II)$. The three platinum atoms were arranged in a linear array with Pt–Pt bond distances of 2.615(1) Å (**13a**), average 2.640 Å (**14a**), and 2.6409(8) Å (**15a**). The outer Pt atoms are coordinated by one isocyanide and one chelating diphosphine, and the central Pt atom is bound only to the two neighboring Pt atoms, resulting in a coordinatively unsaturated platinum center. The coordinatively unsaturated triplatinum complexes **13**–**15** have 40 valence electrons and are extremely electron-deficient. In the electrolysis of **5a**, further reduction led to the formation of a mononuclear hydride complex of platinum, [PtH(dtbpe)(2,6-Me$_2$C$_6$H$_3$NC)]PF$_6$ (**16a**). The potentiostatic electrolysis of **2** consumed 1.5 F mol^{-1} to afford the coordinatively saturated triplatinum complex, [{Pt(dppe)(RNC)}$_2$Pt(RNC)$_2$](PF$_6$)$_2$ (**10**), instead of the unsaturated trimer. The analogous compounds [{Pt(diphos)(RNC)}$_2$Pt(RNC)$_2$](PF$_6$)$_2$ (diphos = dppen (**11**) and dtbpe (**12**)) were also obtained from the reaction of [Pt$_3$(RNC)$_8$]$^{2+}$ with diphosphines. Complex **11a** (R = 2,6-Me$_2$C$_6$H$_3$) crystallizes in the monoclinic system, space group $P2_1/c$, with a = 13.403(3) Å, b = 16.126(4) Å, c = 21.944(8) Å, β = 98.57(2)°, and Z = 2 (R = 0.054 and R_w = 0.040 for 3064 independent reflections with $I > 3\sigma(I)$). The Pt–Pt bond length of 2.655(1) Å is longer by 0.040 Å than that of **13a**. A two-electron reduction of **4** at ca. −1.8 V yielded a Hg–Pt mixed-metal cluster, [HgPt$_6$(dppb)$_2$(RNC)$_8$] (**17**). The length of methylene chain in the diphosphine ligands dramatically influences the structure of the metal–metal bonded platinum clusters. Extended Hückel MO calculations were carried out on the models, [{Pt(PH$_3$)$_2$(HNC)}$_2$Pt]$^{2+}$ and [{Pt(PH$_3$)$_2$(HNC)}$_2$Pt(HNC)$_2$]$^{2+}$, for the coordinatively unsaturated and saturated trimers.

0276-7333/94/2313-1374$04.50/0

Introduction

Polynuclear complexes of platinum and palladium containing metal–metal bonds have been of significant interest because they serve as plausible models for the surface of heterogeneous catalysts and their reactions may mimic those on such surfaces.[2] In homogeneous catalytic reactions, coordinatively unsaturated species play an important role as intermediates, and most of these are thought to be mononuclear. In relevance to heterogeneous catalysts, it is extremely desirable to prepare and characterize polynuclear complexes involving a coordinatively unsaturated metal site, as such complexes would create a new aspect in activation of organic compounds and inert small molecules such as carbon dioxide, dinitrogen, and alkanes. However, such structurally characterized clusters (also including dinuclear complexes) have been extremely limited thus far, e.g., $Pt_2(^tBu_2P(CH_2)_3P^tBu_2)_2$[3] and $[M_3(dppm)_3(CO)]^{2+}$ (M = Pt, Pd; dppm = bis(diphenylphosphino)methane),[4] and clusters that contain a ligand-free metal site (called "naked" metal site) have not been isolated yet. Ligand-free metal clusters can be created in an ultradispersed condensed phase,[5] but they are difficult to isolate and characterize due to their high reactivities.

We have studied the electrochemical preparation of di-, tri-, and polynuclear palladium and platinum complexes of isocyanides (RNC). Electrochemical techniques have many advantages for the preparation of low-valent transition-metal complexes by regulating the potential and the charge consumed. Controlled potential electrolysis of $PtCl_2(RNC)_2$ at a mercury-pool electrode gave $Pt_2Cl_2(RNC)_4$, $Pt_3(RNC)_6$, or $[HgPt_6(RNC)_{12}]$,[6] and that of $[Pt(RNC)_4]^{2+}$ yielded $[Pt_2(RNC)_6]^{2+}$ or $[Pt_3(RNC)_8]^{2+}$,[7,8] depending on the coulometric conditions. By a similar procedure at a platinum-plate electrode, $PdCl_2(RNC)_2$ was readily reduced to the dimer $Pd_2Cl_2(RNC)_4$.[9] Recently, bidentate diphosphines were introduced to the electrochemical system as supporting ligands for the metal–metal bonds. The electroreduction of $[Pt(dppm)(RNC)_2](PF_6)_2$ gave the dppm-bridged dimer $[Pt_2(\mu\text{-dppm})_2(RNC)_2](PF_6)_2$ and the trimetallic A-frame complex $[Pt_3(\mu\text{-dppm})_2(RNC)_4](PF_6)_2{\cdot}CH_2Cl_2$.[7,8] One-electron reduction of $[Pd(diphos)(RNC)_2](PF_6)_2$ (diphos = $Ph_2P(CH_2)_nPPh_2$, n = 2–4) at a platinum-plate electrode afforded the nonbridged dinuclear complex $[Pd_2(diphos)_2(RNC)_2](PF_6)_2$ in which the diphosphines act as chelating ligands.[10]

In this study, *cis*-1,2-bis(diphenylphosphino)ethene (dppen), 1,2-bis(diphenylphosphino)ethane (dppe), 1,3-bis(diphenylphosphino)propane (dppp), 1,4-bis(diphenylphosphino)butane (dppb), and 1,2-bis(di-*tert*-butylphosphino)ethane (dtbpe) were used to elucidate the effects of the length of the methylene chains in diphosphine ligands on the metal–metal bonded structures of platinum compounds. We report unprecedented triplatinum complexes containing a coordinatively unsaturated platinum center, whose bonding structures may reflect those of chemisorbed species on catalytic platinum surfaces. Further, related di-, tri-, and polynuclear platinum complexes containing chelating diphosphine ligands were also prepared by electrochemical techniques. A preliminary account has already been reported.[11]

Experimental Section

All manipulations were carried out under a nitrogen atmosphere. Acetonitrile was distilled over calcium hydride, and $[^nBu_4N][ClO_4]$ was recrystallized from ethyl acetate prior to use. Other reagents were of the best commercial grade and were used without further purification. The isocyanides,[12] *cis*-1,2-bis(diphenylphosphino)ethene,[13] 2-bis(di-*tert*-butylphosphino)ethane,[14] $PtCl_2(COD)$,[15] $[Pt_2(RNC)_6](PF_6)_2$, and $[Pt_3(RNC)_8](PF_6)_2$[7,8] were prepared by known methods.

NMR spectroscopy was carried out on a JEOL EX-400 or a Bruker AC250 instrument at room temperature. ^1H NMR spectra were measured at 400 MHz using tetramethylsilane (TMS) as an internal reference, and $^{31}P\{^1H\}$ NMR spectra were measured at 100 MHz in CD_2Cl_2 using H_3PO_4 as an external reference. Infrared and electronic absorption spectra were recorded on Jasco FT/IR-5300 and Ubest-30 spectrometers, respectively. Cyclic voltammetry and potentiostatic electrolysis were carried out using a HUSO 956B potentiostat and a HUSO 321 potential scanning unit. The electrolytic cell consisted of a conventional three-electrode system, a platinum-button electrode (1.6-mm i.d.) as a working electrode, a Pt wire as a counter electrode, and a $Ag/AgNO_3$ (0.1 M)–0.1 M $[^nBu_4N][ClO_4]$/MeCN system as a reference electrode, for recording cyclic voltammograms. In the bulk electrolysis, a mercury-pool electrode was used as a working electrode, and the counter electrode was separated by a glass filter. All potentials were calibrated relative to the Cp_2Fe/Cp_2Fe^+ (1.0 mM in MeCN) redox couple.

Preparation of $[Pt(diphos)(RNC)_2](PF_6)_2$ (diphos = dppen (1), dppe (2), dppp (3), dppb (4), and dtbpe (5)). As a typical procedure, dppe (2.0 mmol), 2,6-$Me_2C_6H_3NC$ (4.0 mmol), and an excess of NH_4PF_6 (10.0 mmol) were successively added to a solution of CH_2Cl_2 (30 mL) and acetone (30 mL) containing 2.0 mmol of $PtCl_2(COD)$. The solution was stirred at room temperature for 2 h, and then the solvent was removed to dryness under reduced pressure. The residue was extracted with CH_2Cl_2 (ca. 60 mL), washed with H_2O (ca. 20 mL), and dried over Na_2SO_4. The resultant solution was concentrated to ca. 20 mL, and addition of diethyl ether gave pale yellow crystals of $[Pt(dppe)(2,6\text{-}Me_2C_6H_3NC)_2](PF_6)_2{\cdot}0.5CH_2Cl_2$ (**2a**): yield 84%. Anal. Calcd for $C_{44}H_{42}N_2PtP_4F_{12}{\cdot}0.5CH_2Cl_2$: C, 44.98; H, 3.65; N, 2.36. Found: C, 44.85; H, 3.86; N, 2.36. IR (Nujol): $\nu_{N\equiv C}$ 2219 cm^{-1}. UV–vis (CH_2Cl_2): λ_{max} (log ϵ) 299 (4.17) nm. ^1H NMR (acetone-d_6): δ 2.15 (s, *o*-Me), 3.40 (m, CH_2), 5.30 (s, CH_2Cl_2), 7.2–8.3 (m, Ar). $[Pt(dppen)(2,6\text{-}Me_2C_6H_3NC)_2](PF_6)_2{\cdot}0.5CH_2Cl_2$ (**1a**): yield 87%. Anal. Calcd for $C_{44}H_{40}N_2PtP_4F_{12}{\cdot}0.5CH_2Cl_2$: C, 45.06; H,

• Abstract published in *Advance ACS Abstracts*, March 1, 1994.

(1) (a) Electrochemical studies of organometallic compounds. 10. Part 9: Tanase, T.; Kawahara, K.; Ukaji, H.; Kobayashi, K.; Yamazaki, H.; Yamamoto, Y. *Inorg. Chem.* **1993**, *32*, 3682. (b) RIKEN (Institute of Physical and Chemical Research), Wako, Saitama 351, Japan.

(2) (a) Muetterties, E. L. *Bull. Soc. Chim. Belg.* **1976**, *85*, 451. (b) Muetterties, E. L.; Rhodin, T. N.; Band, E.; Brucker, C. F.; Pretzer, W. R. *Chem. Rev.* **1979**, *79*, 91.

(3) Yoshida, T.; Yamagata, T.; Tulip, T. H.; Ibers, J. A.; Otsuka, S. *J. Am. Chem. Soc.* **1978**, *100*, 2063.

(4) (a) Manojlovic-Muir, Lj.; Muir, K. W.; Lloyd, B. R.; Pudephatt, R. J. *J. Chem. Soc., Chem. Commun.* **1983**, 1336. (b) Lloyd, B. R.; Puddephatt, R. J. *Inorg. Chim. Acta* **1984**, *90*, L77. (c) Manojlovic-Muir, Lj.; Muir, K. W.; Lloyd, B. R.; Pudephatt, R. J. *J. Chem. Soc., Chem. Commun.* **1985**, 536. (d) Ferguson, G.; Lloyd, B. R.; Puddephatt, R. J. *Organometallics* **1986**, *5*, 344.

(5) Davis, S. C.; Klabunde, K. J. *Chem. Rev.* **1982**, *82*, 153.

(6) (a) Kamamoto, Y.; Takahashi, K.; Matsuda, K.; Yamazaki, H. *J. Chem. Soc., Dalton Trans.* **1987**, 1833. (b) Yamamoto, Y.; Takahashi, K.; Yamazaki, H. *Chem. Lett.* **1985**, 201.

(7) Yamamoto, Y.; Takahashi, K.; Yamazaki, H. *J. Am. Chem. Soc.* **1986**, *108*, 2458.

(8) Yamamoto, Y.; Yamazaki, H. *Organometallics* **1993**, *12*, 933.

(9) Yamamoto, Y.; Takahashi, K.; Yamazaki, H. *Bull. Chem. Soc. Jpn.* **1987**, *60*, 2665.

(10) Tanase, T.; Kawahara, K.; Ukaji, H.; Kobayashi, K.; Yamazaki, H.; Yamamoto, Y. *Inorg. Chem.* **1993**, *32*, 3682.

(11) Tanase, T.; Kudo, Y.; Ohno, M.; Kobayashi, K.; Yamamoto, Y. *Nature* **1990**, *344*, 526.

(12) (a) Walborsky, H. M.; Niznik, G. E. *J. Org. Chem.* **1972**, *37*, 187. (b) Yamamoto, Y.; Aoki, K.; Yamazaki, H. *Inorg. Chem.* **1979**, *18*, 1681.

(13) Aguiar, A. M.; Daigle, D. *J. Am. Chem. Soc.* **1964**, *86*, 2299.

(14) Yamagata, T. (Osaka University). Private communication.

(15) Chatt, J.; Vallarino, L. M.; Venanzi, L. M. *J. Chem. Soc.* **1957**, 2496.

3.48; N, 2.36. Found: C, 45.58; H, 3.33; N, 2.34. IR (Nujol): $\nu_{N\equiv C}$ 2220 cm^{-1}. UV-vis (CH_2Cl_2): λ_{max} (log ϵ) 240 (4.72) nm. ^{1}H NMR (acetone-d_6): δ 2.23 (s, *o*-Me), 5.30 (s, CH_2Cl_2), 7.2–8.2 (m, Ar and HC=CH). [Pt(dppen)(2,4,6-$Me_3C_6H_2NC)_2$]$(PF_6)_2$·0.5CH_2Cl_2 (**1b**): yield 72%. Anal. Calcd for $C_{46}H_{44}N_2PtP_4F_{12}$·0.5$CH_2Cl_2$: C, 45.99; H, 3.74; N, 2.31. Found: C, 46.31; H, 3.40; N, 2.11. IR (Nujol): $\nu_{N\equiv C}$ 2212 cm^{-1}. UV-vis (CH_2Cl_2): λ_{max} (log ϵ) 234 (2.59), 269 (4.41) nm. ^{1}H NMR (acetone-d_6): δ 2.06 (s, *o*-Me), 2.31 (s, *p*-Me), 5.30 (s, CH_2Cl_2), 6.9–7.9 (m, Ar and HC=CH). [Pt(dppe)(2,4,6-$Me_3C_6H_2NC)_2$]$(PF_6)_2$·CH_2Cl_2 (**2b**): yield 64%. Anal. Calcd for $C_{46}H_{46}N_2PtP_4F_{12}$·$CH_2Cl_2$: C, 44.85; H, 3.84; N, 2.23. Found: C, 45.34; H, 4.06; N, 2.24. IR (Nujol): $\nu_{N\equiv C}$ 2217 cm^{-1}. UV-vis (CH_2Cl_2): λ_{max} (log ϵ) 304 (4.39) nm. ^{1}H NMR (acetone-d_6): δ 2.08 (s, *o*-Me), 2.29 (s, *p*-Me), 3.40 (m, CH_2), 5.30 (s, CH_2Cl_2), 7.0–8.3 (m, Ar). [Pt(dppp)(2,6-$Me_2C_6H_3NC)_2$]$(PF_6)_2$ (**3a**): yield 99%. Anal. Calcd for $C_{45}H_{44}N_2PtP_4F_{12}$: C, 46.60; H, 3.82; N, 2.42. Found: C, 46.80; H, 3.90; N, 2.36. IR (Nujol): $\delta_{N\equiv C}$ 2214 cm^{-1}. UV-vis (CH_2Cl_2): λ_{max} (log ϵ) 298^{sh} (4.03) nm. ^{1}H NMR (acetone-d_6): δ 2.14 (s, *o*-Me), 2.5–3.5 (br, CH_2), 7.0–8.0 (m, Ar). [Pt(dppp)(2,4,6-$Me_3C_6H_2NC)_2$]$(PF_6)_2$ (**3b**): yield 99%. Anal. Calcd for $C_{47}H_{48}N_2PtP_4F_{12}$: C, 47.52; H, 4.07; N, 2.36. Found: C, 47.68; H, 3.70; N, 2.13. IR (Nujol): $\nu_{N\equiv C}$ 2232 cm^{-1}. UV-vis (CH_2Cl_2): λ_{max} (log ϵ) 299^{sh} (4.13) nm. ^{1}H NMR (acetone-d_6): δ 2.09 (s, *o*-Me), 2.28 (s, *p*-Me) 2.4–3.5 (m, CH_2), 6.9–8.1 (m, Ar). [Pt(dppb)(2,6-$Me_2C_6H_3NC)_2$]$(PF_6)_2$·0.5CH_2Cl_2 (**4a**): yield 96%. Anal. Calcd for $C_{46}H_{46}N_2PdP_4F_{12}$·0.5$CH_2Cl_2$: C, 45.92; H, 3.89; N, 2.30. Found: C, 46.81; H, 3.39; N, 2.18. IR (Nujol): $\nu_{N\equiv C}$ 2209 cm^{-1}. UV-vis (CH_2Cl_2): λ_{max} (log ϵ) 296^{sh} (3.76) nm. ^{1}H NMR (DMSO-d_6): δ 2.01 (s, *o*-Me), 2.8–3.5 (m, CH_2), 5.74 (s, CH_2Cl_2), 6.8–8.0 (m, Ar). [Pt(dppb)(2,4,6-$Me_3C_6H_2$-$NC)_2$]$(PF_6)_2$ (**4b**): yield 90%. Anal. Calcd for $C_{48}H_{50}N_2$-PtP_4F_{12}: C, 47.97; H, 4.19; N, 2.33. Found: C, 47.69; H, 3.76; N, 2.14. IR (Nujol): $\nu_{N\equiv C}$ 2213 cm^{-1}. ^{1}H NMR (DMSO-d_6): δ 1.95 (s, *o*-Me), 2.15 (s, *p*-Me), 2.7–3.7 (m, CH_2), 6.7–8.1 (m, Ar). [Pt(dtbpe)(2,6-$Me_2C_6H_3NC)_2$]$(PF_6)_2$ (**5a**): yield 97%. Anal. Calcd for $C_{36}H_{58}N_2PtP_4F_{12}$: C, 40.57; H, 5.48; N, 2.63. Found: C, 40.84; H, 5.09; N, 3.17. IR (Nujol): $\nu_{N\equiv C}$ 2210, 2196 cm^{-1}. UV-vis (CH_2Cl_2): λ_{max} (log ϵ) 297 (4.17), 246 (4.47) nm. ^{1}H NMR (acetone-d_6): δ 1.69 (d, ^{t}Bu–P, J_{PH} = 15.6 Hz), 2.57 (s, *o*-Me), 2.90 (d, CH_2, J_{PH} = 12.7 Hz), 7.36–7.50 (m, Ar). [Pt(dtbpe)(2,4,6-$Me_3C_6H_2NC)_2$]$(PF_6)_2$ (**5b**): yield 77%. Anal. Calcd for $C_{38}H_{62}N_2PtP_4F_{12}$: C, 41.72; H, 5.71; N, 2.56. Found: C, 42.15; H, 5.80; N, 2.42. IR (Nujol): $\nu_{N\equiv C}$ 2214, 2200 cm^{-1}. UV-vis (CH_2Cl_2): λ_{max} (log ϵ) 300 (4.09), 253 (4.58) nm. ^{1}H NMR (CD_2-Cl_2): δ 1.55 (d, ^{t}Bu–P, J_{PH} = 15.6 Hz), 2.35 (s, *p*-Me), 2.44 (s, *o*-Me), 2.55 (d, CH_2, J_{PH} = 12.2 Hz), 7.05 (s, Ar).

Electrochemical Preparation of [Pt_2(diphos)$_2$(RNC)$_2$]-$(PF_6)_2$ (diphos = dppen (6), dppe (7), dppp (8), dppb (9)). [Pt(diphos)$(RNC)_2$]$(PF_6)_2$ (1–4) (0.2 mmol) was dissolved in 30 mL of a 0.1 M acetonitrile solution of $NaClO_4$. After passage of the appropriate amount of charge (1 F mol^{-1}) at −1.45 to −1.50 V by using a mercury-pool electrode, the solution was separated by decantation and the solvent was removed under reduced pressure. The residue was extracted with CH_2Cl_2 (30 mL) and concentrated to ca. 10 mL, and addition of diethyl ether gave yellow crystals of [Pt_2(diphos)$_2(RNC)_2$]$(PF_6)_2$ (6–9), which were recrystallized from a CH_2Cl_2/Et_2O or a CH_3CN/Et_2O mixed solvent. [Pt_2(dppen)$_2$(2,6-$Me_2C_6H_3NC)_2$]$(PF_6)_2$·2CH_2Cl_2 (**6a**): yield 55%. Anal. Calcd for $C_{70}H_{62}N_2Pt_2P_6F_{12}$·2$CH_2Cl_2$: C, 45.39; H, 3.49; N, 1.47. Found: C, 46.38; H, 3.07; N, 1.41. IR (Nujol): $\nu_{N\equiv C}$ 2155 cm^{-1}. UV-vis (CH_2Cl_2): λ_{max} (log ϵ) 315^{sh} (4.08) nm. ^{1}H NMR (acetone-d_6): δ 1.95 (s, *o*-Me), 5.30 (s, CH_2Cl_2), 7.2–8.2 (m, CH=CH and Ar). [Pt_2(dppen)$_2$(2,4,6-$Me_3C_6H_2NC)_2$]-$(PF_6)_2$·0.5CH_2Cl_2 (**6b**): yield 55%. Anal. Calcd for $C_{72}H_{66}N_2Pt_2P_6F_{12}$·0.5$CH_2Cl_2$: C, 48.22; H, 3.74; N, 1.55. Found: C, 48.98; H, 3.25; N, 1.40. IR (Nujol): $\nu_{N\equiv C}$ 2149 cm^{-1}. UV-vis (CH_2Cl_2): λ_{max} (log ϵ) 310^{sh} (4.16) nm. ^{1}H NMR (CD_2Cl_2): δ 1.76 (s, *o*-Me), 2.31 (s, *p*-Me), 5.30 (s, CH_2Cl_2), 6.7–7.7 (m, Ar and CH=CH). [Pt_2(dppe)$_2$(2,6-$Me_2C_6H_3NC)_2$]$(PF_6)_2$ (**7a**): yield 22%. Anal. Calcd for $C_{70}H_{66}N_2Pt_2P_6F_{12}$: C, 48.34; H, 3.82; N, 1.61. Found: C, 48.02; H, 3.79; N, 1.54. IR (Nujol): $\nu_{N\equiv C}$ 2152 cm^{-1}. UV-vis (CH_2Cl_2): λ_{max} (log ϵ) 322 (4.19) nm. ^{1}H NMR (acetone-d_6): δ 2.07 (s, *o*-Me), 1.8–3.5 (m, CH_2), 6.8–8.0 (m, Ar). [Pt_2(dppe)$_2$(2,4,6-$Me_3C_6H_2NC)_2$]$(PF_6)_2$ (**7b**): yield 83%. Anal. Calcd for $C_{72}H_{70}N_2Pt_2P_6F_{12}$: C, 48.93; H, 3.99; N, 1.59. Found: C, 48.67; H, 3.98; N, 1.72. IR (Nujol): $\nu_{N\equiv C}$ 2171 cm^{-1}. UV-vis (CH_2Cl_2): λ_{max} (log ϵ) 321 (4.23) nm. ^{1}H NMR (acetone-d_6): δ 2.04 (s, *o*-Me), 2.36 (s, *p*-Me), 1.8–3.5 (m, CH_2), 6.8–8.0 (m, Ar). [Pt_2(dppp)$_2$(2,6-$Me_2C_6H_3NC)_2$]$(PF_6)_2$ (**8a**): yield 19%. Anal. Calcd for $C_{72}H_{70}N_2Pt_2P_6F_{12}$: C, 48.93; H, 3.99; N, 1.59. Found: C, 48.98; H, 4.01; N, 1.73. IR (Nujol): $\nu_{N\equiv C}$ 2143 cm^{-1}. UV-vis (CH_2Cl_2): λ_{max} (log ϵ) 322 (4.14) nm. ^{1}H NMR (acetone-d_6): δ 1.94 (s, *o*-Me), 1.2–3.1 (m, CH_2), 6.4–8.1 (m, Ar). [Pt_2(dppp)$_2$(2,4,6-$Me_3C_6H_2NC)_2$]$(PF_6)_2$ (**8b**): yield 55%. Anal. Calcd for $C_{74}H_{74}N_2Pt_2P_6F_{12}$: C, 49.51; H, 4.15; N, 1.56. Found: C, 48.95; H, 4.09; N, 1.62. IR (Nujol): $\nu_{N\equiv C}$ 2149 cm^{-1}. UV-vis (CH_2Cl_2): λ_{max} (log ϵ) 321 (4.17) nm. ^{1}H NMR (CD_2Cl_2): δ 1.67 (s, *o*-Me), 2.35 (s, *p*-Me), 1.0–3.2 (m, CH_2), 6.3–8.0 (m, Ar). [Pt_2(dppb)$_2$(2,6-$Me_2C_6H_3NC)_2$]$(PF_6)_2$·CH_3CN (**9a**): yield 89%. Anal. Calcd for $C_{74}H_{74}N_2Pt_2P_6F_{12}$·$CH_3CN$: C, 49.71; H, 4.23; N, 2.29. Found: C, 49.79; H, 4.16; N, 2.46. IR (Nujol): $\nu_{N\equiv C}$ 2152 cm^{-1}. UV-vis (CH_2Cl_2): λ_{max} (log ϵ) 319 (4.34) nm. ^{1}H NMR (acetone-d_6): δ 2.01 (s, *o*-Me), 1.2–3.3 (m, CH_2), 6.9–8.0 (m, Ar). [Pt_2(dppb)$_2$(2,4,6-$Me_3C_6H_2NC)_2$]$(PF_6)_2$·CH_3CN (**9b**): yield 87%. Anal. Calcd for $C_{76}H_{78}N_2Pt_2P_6F_{12}$·$CH_3CN$: C, 50.25; H, 4.38; N, 2.25. Found: C, 51.01; H, 4.30; N, 2.02. IR (Nujol): $\nu_{N\equiv C}$ 2151 cm^{-1}. UV-vis (CH_2Cl_2): λ_{max} (log ϵ) 316^{sh} (4.41) nm. ^{1}H NMR (acetone-d_6): δ 1.96 (s, *o*-Me), 2.35 (s, *p*-Me), 1.2–3.3 (m, CH_2), 6.9–8.1 (m, Ar).

Electrochemical Preparation of [{Pt(dppe)(RNC)}$_2$Pt-(RNC)$_2$](PF$_6$)$_2$ (10). [Pt(dppe)$(RNC)_2$[$(PF_6)_2$ (2) (0.2 mmol) was dissolved in 30 mL of a 0.1 M acetonitrile solution of $NaClO_4$. After passage of the appropriate amount of charge (1.5 F mol^{-1}) at ca. −1.8 V, the solution was separated by decantation and the solvent was removed under reduced pressure. The residue was extracted with CH_2Cl_2 (30 mL) and concentrated to ca. 10 mL, and addition of diethyl ether gave reddish orange crystals of [{Pt(dppe)(RNC)}$_2$Pt$(RNC)_2$[$(PF_6)_2$ (**10**). [{Pt(dppe)(2,6-$Me_2C_6H_3NC)$}$_2$Pt(2,6-$Me_2C_6H_3NC)_2$]$(PF_6)_2$·0.5CH_2Cl_2 (**10a**): yield 70%. Anal. Calcd for $C_{88}H_{84}N_4Pt_3P_6F_{12}$·0.5$CH_2Cl_2$: C, 47.47; H, 3.83; N, 2.50. Found: C, 47.53; H, 3.82; N, 2.29. IR (Nujol): $\nu_{N\equiv C}$ 2155 cm^{-1}. UV-vis (CH_2Cl_2): λ_{max} (log ϵ) 408 (4.14), 374 (3.89), 337 (4.14), 287 (4.23) nm. ^{1}H NMR (CD_2Cl_2): δ 1.86, 2.25 (s, *o*-Me), 2.5–2.6 (m, CH_2), 5.30 (s, CH_2Cl_2), 6.8–8.1 (m, Ar). [{Pt(dppe)(2,4,6-$Me_3C_6H_2NC)$}$_2$Pt(2,4,6-$Me_3C_6H_2NC)_2$]-$(PF_6)_2$·2CH_2Cl_2 (**10b**): yield 19%. Anal. Calcd for $C_{92}H_{92}N_4Pt_3P_6F_{12}$·2$CH_2Cl_2$: C, 46.60; H, 3.99; N, 2.31. Found: C, 46.60; H, 4.16; N, 2.38. IR (Nujol): $\nu_{N\equiv C}$ 2116 cm^{-1}. UV-vis (CH_2Cl_2): λ_{max} (log ϵ) 408 (4.29), 373 (4.04), 339 (4.36) nm. ^{1}H NMR (CD_2Cl_2): δ 1.64, 2.01 (s, *o*-Me), 2.25, 2.35 (s, *p*-Me), 2.1–2.4 (m, CH_2), 5.30 (s, CH_2Cl_2), 6.6–7.7 (m, Ar).

Preparation of [{Pt(diphos)(RNC)}$_2$Pt(RNC)$_2$](PF$_6$)$_2$ (diphos = dppen (11) and dtbpe (12)). To a dichloromethane solution (20 mL) of [$Pt_3(RNC)_8$]$(PF_6)_2$ (0.1 mmol) was added 0.2 mmol of diphosphines (dppen or dtbpe) in CH_2Cl_2, and the mixture was stirred at room temperature for 30 min. The solution was concentrated to ca. 10 mL, and an addition of diethyl ether gave orange crystals of [{Pt(diphos)(RNC)}$_2$Pt$(RNC)_2$](PF$_6$) (diphos = dppen (11), dtbpe (12)), which were recrystallized from a CH_2Cl_2/Et_2O or an acetone/Et_2O mixed solvent. [{Pt(dppen)(2,6-$Me_2C_6H_3NC)$}$_2$Pt(2,6-$Me_2C_6H_3NC)_2$]$(PF_6)_2$·$(CH_3)_2CO$ (**11a**): yield 65%. Anal. Calcd for $C_{88}H_{80}N_4Pt_3P_6F_{12}$·$C_3H_6O$: C, 48.56; H, 3.85; N, 2.49. Found: C, 48.93; H, 3.48; N, 2.28. IR (Nujol): $\nu_{N\equiv C}$ 2141, 2112 cm^{-1}. UV-vis (CH_2Cl_2): λ_{max} (log ϵ) 455^{sh} (3.70), 403 (4.27), 373 (4.12), 338 (4.36), 290 (4.43), 278 (4.40) nm. ^{1}H NMR (CD_2Cl_2): δ 1.89, 1.90 (s, *o*-Me), 6.8–7.7 (m, Ar and CH=CH). [{Pt(dppen)(2,4,6-$Me_3C_6H_2NC)$}$_2$Pt(2,4,6-$Me_3C_6H_2$-$NC)_2$]$(PF_6)_2$ (**11b**): yield 72%. Anal. Calcd for $C_{92}H_{88}N_4$-$Pt_3P_6F_{12}$: C, 49.14; H, 3.94; N, 2.49. Found: C, 49.06; H, 3.20; N, 2.29. IR (Nujol): $\nu_{N\equiv C}$ 2122 cm^{-1}. UV-vis (CH_2Cl_2): λ_{max} (log ϵ) 402 (4.10), 370 (3.92), 339 (4.24), 292 (4.27) nm. ^{1}H NMR (CD_2Cl_2): δ 1.84 (s, *o*-Me), 2.31, 2.33 (s, *p*-Me), 6.8–7.7 (m, Ar and CH=CH). [{Pt(dtbpe)(2,6-$Me_2C_6H_3NC)$}$_2$Pt(2,6-$Me_2C_6H_3NC)_2$]-$(PF_6)_2$·0.5CH_2Cl_2 (**12a**): yield 15%. Anal. Calcd for $C_{72}H_{116}N_4Pt_3P_6F_{12}$·0.5$CH_2Cl_2$: C, 41.88; H, 5.67; N, 2.69. Found:

Table 1. Crystallographic and Experimental Data for 8b, 11a, 16a, 13a, 14a, and 15a

	8b	11a	16a	13a	14a	15a
formula	$C_{74}H_{74}N_2PtP_6F_{12}$	$C_{94}H_{92}N_4Pt_3P_6F_{12}O_2$	$C_{27}H_{50}NPtP_3F_6$	$C_{74}H_{68}N_4Pt_3P_6F_{12}$	$C_{72}H_{70}N_2Pt_3P_6F_{12}$	$C_{54}H_{98}N_2Pt_3P_6F_{12}$
fw	1795.42	2308.88	790.70	2012.47	1962.42	1774.47
cryst syst	monoclinic	monoclinic	triclinic	monoclinic	monoclinic	monoclinic
space group	$P2_1/c$ (No. 14)	$P2_1/c$ (No. 14)	$P\bar{1}$ (No. 2)	$P2/n$ (No. 13)	$P2_1$ (No. 4)	$C2/c$ (No. 15)
lattice const						
a, Å	14.941(4)	13.403(3)	13.378(2)	14.956(4)	15.491(3)	19.489(6)
b, Å	19.268(6)	16.126(4)	14.909(4)	12.395(2)	22.575(5)	15.284(5)
c, Å	26.002(9)	21.944(8)	8.701(4)	22.923(7)	10.884(3)	25.804(6)
α, deg			103.61(3)			
β, deg	101.23(2)	98.57(2)	95.53(3)	104.35(2)	107.48(2)	116.34(2)
γ, deg			86.86(2)			
V, Å^3	7342	4690	1678	4117	3630	6888
Z	4	2	2	2	2	4
2θ limit, deg	55	45	50	45	52	50
scan method	ω–2θ	ω–2θ	ω–2θ	ω–2θ	ω ($2\theta < 30°$), θ–2θ ($30° < 2\theta < 52°$)	ω–2θ
scan speed, deg min^{-1}	4	16	16	16	4	16
T, °C	23	23	23	23	23	23
D_{calcd}, g cm^{-3}	1.624	1.635	1.565	1.623	1.796	1.711
μ, mm^{-1}	4.05	4.68	4.41	5.32	6.03	6.34
no. of obsd data	7804	4623	5906	3541	5009	6324
no. of unique data	5704 ($I > 3\sigma(I)$)	3064 ($I > 3\sigma(I)$)	3662 ($I > 3\sigma(I)$)	2872 ($I > 3\sigma(I)$)	3156 ($I > 3\sigma(I)$)	2904 ($I > 3\sigma(I)$)
no. of params	866	527	343	448	486	348
data/param	6.59	5.81	10.68	6.41	6.49	8.34
R^a	0.059	0.054	0.044	0.048	0.056	0.045
$R_w{}^b$	0.051	0.040	0.035	0.046	0.038	0.033
GOF	1.64	1.31	1.25	1.52	1.45	1.20

^{a} $R = \sum||F_o| - |F_c||/\sum|F_o|$. ^{b} $R_w = [\sum w(|F_o| - |F_c|)^2/\sum w|F_o|^2]^{1/2}$ ($w = 1/\sigma^2(F_o)$).

C, 42.00; H, 5.26; N, 2.59. IR (Nujol): $\nu_{N\equiv C}$ 2114, 2089 cm^{-1}. UV–vis (CH_2Cl_2): λ_{max} (log ϵ) 404 (3.80), 335 (3.92) nm.

Electrochemical Preparation of [{Pt(diphos)(RNC)}$_2$Pt](PF$_6$)$_2$ (diphos = dppen (13) and dppp (14)). [Pt(dppen)(RNC)$_2$](PF$_6$)$_2$ (1) (0.2 mmol) was dissolved in 30 mL of a 0.1 M acetonitrile solution of $NaClO_4$. After passage of the appropriate amount of charge (1.5 F mol^{-1}) at ca. −1.8 V, the solution was separated by decantation and the solvent was removed under reduced pressure. The residue was extracted with CH_2Cl_2 (30 mL) and concentrated to ca. 10 mL, and addition of diethyl ether gave yellow crystals of 6 (8–10%). A further crystallization from the mother liquor afforded orange-yellow crystals of [{Pt(dppen)(RNC)}$_2$Pt](PF$_6$)$_2$ (13) and a trace amount of reddish orange crystals of 11. [{Pt(dppen)(2,6-Me$_2$C$_6$H$_3$NC)}$_2$Pt](PF$_6$)$_2$·CH_2Cl_2 (13a): yield 12%. Anal. Calcd for $C_{70}H_{62}N_2Pt_3P_6F_{12}$·$CH_2Cl_2$: C, 42.32; H, 3.20; N, 1.39. Found: C, 43.56; H, 2.55; N, 1.30. IR (Nujol): $\nu_{N\equiv C}$ 2141 cm^{-1}. UV–vis (CH_2Cl_2): λ_{max} (log ϵ) 466^{sh} (2.99), 372 (4.08), 335 (3.85), 296 (4.14) nm. ^{1}H NMR (CD_2Cl_2): δ 1.96 (s, *o*-Me), 5.30 (s, CH_2Cl_2), 7.0–7.7 (m, CH=CH and Ar). [{Pt(dppen)(2,4,6-Me$_3$C$_6$H$_2$NC)}$_2$Pt](PF$_6$)$_2$·CH_2Cl_2 (13b): yield 19%. Anal. Calcd for $C_{72}H_{66}N_2Pt_3P_6F_{12}$·$CH_2Cl_2$: C, 42.91; H, 3.35; N, 1.37. Found: C, 42.33; H, 3.57; N, 1.65. IR (Nujol): $\nu_{N\equiv C}$ 2143 cm^{-1}. UV–vis (CH_2Cl_2): λ_{max} (log ϵ) 470^{sh} (3.01), 375 (3.99), 336 (3.69), 303 (4.04), 277^{sh} (4.01) nm. ^{1}H NMR (CD_2Cl_2): δ 1.91 (s, *o*-Me), 2.33 (s, *p*-Me), 5.30 (s, CH_2Cl_2), 6.90 (s, *m*-H), 7.2–7.7 (m, Ar and CH=CH).

A similar electrolysis of 3 (0.2 mmol) at ca. −1.8 V and the concomitant workup gave orange crystals of [{Pt(dppp)(RNC)}$_2$Pt](PF$_6$)$_2$ (14) and yellow crystals of 7 (30–40%). [{Pt(dppp)(2,6-Me$_2$C$_6$H$_3$)}$_2$Pt](PF$_6$)$_2$ (14a): yield 11%. Anal. Calcd for $C_{72}H_{70}N_2Pt_3P_6F_{12}$: C, 44.07; H, 3.60; N, 1.43. Found: C, 44.55; H, 3.74; N, 1.56. IR (Nujol): $\nu_{N\equiv C}$ 2141 cm^{-1}. UV–vis (CH_2Cl_2): λ_{max} (log ϵ) 363 (4.20), 343^{sh} (4.04), 301 (4.16) nm. ^{1}H NMR (CD_2Cl_2): δ 2.00 (s, *o*-Me), 2.7–3.0 (br, CH_2), 6.8–7.8 (m, Ar). [{Pt(dppp)(2,4,6-Me$_3$C$_6$H$_2$)}$_2$Pt](PF$_6$)$_2$ (14b): yield 8%. Calcd for $C_{74}H_{74}N_2Pt_3P_6F_{12}$: C, 44.65; H, 3.75; N, 1.41. Found: C, 44.63; H, 3.85; N, 1.50. IR (Nujol): $\nu_{N\equiv C}$ 2135 cm^{-1}. UV–vis (CH_2Cl_2): λ_{max} (log ϵ) 363 (4.18), 304 (4.25) nm. ^{1}H NMR (CD_2Cl_2): δ 1.89 (s, *o*-Me), 2.38 (s, *p*-Me), 2.7–3.0 (br, CH_2), 6.5–7.9 (m, Ar).

Electrochemical Preparation of [{Pt(dtbpe)(RNC)}$_2$Pt](PF$_6$)$_2$ (15) and [PtH(dtbpe)(RNC)]PF$_6$ (16). [Pt(dtbpe)(2,6-Me$_2$C$_6$H$_3$NC)$_2$](PF$_6$)$_2$ (5a) (0.2 mmol) was dissolved in 30 mL of a 0.1 M acetonitrile solution of $NaClO_4$. After passage of the appropriate amount of charge (1.5 F mol^{-1}) at ca. −1.8 V, the solution was separated by decantation and the solvent was removed under reduced pressure. The residue was extracted with CH_2Cl_2 (30 mL) and concentrated to ca. 10 mL, and addition of diethyl ether gave a mixture of yellow crystals of [{Pt(dtbpe)(2,6-Me$_2$C$_6$H$_3$NC)}$_2$Pt](PF$_6$)$_2$ (15a) and white crystals of [PtH(dtbpe)(2,6-Me$_2$C$_6$H$_3$NC)]PF$_6$ (16a). The mixture was washed with a small amount of THF (10 mL), and the residue was recrystallized from a CH_2Cl_2/Et_2O mixed solvent to give [{Pt(dtbpe)(RNC)}$_2$Pt](PF$_6$)$_2$ (15a): yield 13%. Anal. Calcd for $C_{54}H_{78}N_2Pt_3P_6F_{12}$: C, 36.55; H, 5.57; N, 1.58. Found: C, 37.01; H, 5.53; N, 1.35. IR (Nujol): $\nu_{N\equiv C}$ 2137 cm^{-1}. UV–vis (CH_2Cl_2): λ_{max} (log ϵ) 323 (4.22), 302 (4.09) nm. ^{1}H NMR (CD_2Cl_2): δ 1.36 (d, ^{t}Bu–P, J_{PH} = 14.1 Hz), 1.44 (d, ^{t}Bu–P, J_{PH} = 14.1 Hz), 2.3–2.5 (m, CH_2), 2.56 (s, *o*-Me), 7.3–7.5 (m, Ar). Addition of Et_2O to the THF washing afforded colorless crystals of 16a: yield 32%. Anal. Calcd for $C_{27}H_{50}NPtP_3P_6$: C, 41.01; H, 6.37; N, 1.77. Found: C, 40.75; H, 6.34; N, 1.70. IR (Nujol): $\nu_{N\equiv C}$ 2166, ν_{PtH} 2031 cm^{-1}. UV–vis (CH_2Cl_2): λ_{max} (log ϵ) 320 (3.48), 284 (4.12), 267 (4.15) nm. ^{1}H NMR ($CDCl_3$): δ −2.85 (dd, H–Pt, J_{PtH} = 911.7 Hz, $J_{P(trans)H}$ = 161.5 Hz, $J_{P(cis)H}$ = 12.4 Hz), 1.45 (d, ^{t}Bu–P, J_{PH} = 12.2 Hz), 1.48 (d, ^{t}Bu–P, J_{PH} = 11.8 Hz), 2.3–2.6 (m, CH_2), 2.53 (s, *o*-Me), 7.3–7.5 (m, Ar).

Crystal Data and Intensity Measurements for [Pt$_2$(dppp)$_2$(2,4,6-Me$_3$C$_6$H$_2$NC)$_2$](PF$_6$)$_2$ (8b), [{Pt(dppen)(2,6-Me$_2$C$_6$H$_3$NC)}$_2$Pt](PF$_6$)$_2$·2CH$_3$CN (13a), [{Pt(dppp)(2,6-Me$_2$C$_6$H$_3$NC)}$_2$Pt](PF$_6$)$_2$ (14a), [{Pt(dtbpe)(2,6-Me$_2$C$_6$H$_3$NC)}$_2$Pt](PF$_6$)$_2$ (15a), [PtH(dtbpe)(2,6-Me$_2$C$_6$H$_3$NC)]PF$_6$ (16a), and [{Pt(dppen)(2,6-Me$_2$C$_6$H$_3$NC)}$_2$Pt(2,6-Me$_2$C$_6$H$_3$NC)$_2$](PF$_6$)$_2$·2(CH$_3$)$_2$CO (11a). Suitable crystals were obtained by recrystallizations from CH_2Cl_2/Et_2O (8b, 14a, 15a), CH_3CN/Et_2O (13a, 16a), and $(CH_3)_2CO$/Et_2O (11a) mixed solvents. Crystal data and experimental conditions for 8b, 11a, 13a, 14a, 15a, and 16a are listed in Table 1. Crystals sealed into a 0.7-mm-i.d. glass-tube capillary were used in the intensity data collection on a Rigaku four-circle automated diffractometer, AFC5S (8b, 11a, 13a, 15a, and 16a) or AFC4 (14a), equipped with Mo Kα radiation. Three standard reflections were monitored every 150 reflections and showed no systematic decrease in intensity. Totals of 7804 (8b), 3541 (13a), 7713 (14a), 6324 (15a), 5906 (16a), and 4623 reflections (11a) were measured, and the intensities were collected for Lorentz-polarization effects. Absorption corrections by the ψ-scan method were applied.

Structure Solution and Refinement.[16] Compounds 8b and 15a. The structure was solved by direct methods with MITHRIL.[17] The two platinum atoms were located in the initial E map, and subsequent Fourier syntheses gave the positions of other non-hydrogen atoms. The coordinates of all hydrogen atoms were calculated at ideal positions with a C–H distance of 0.95 Å and were not refined. The structure was refined with full-matrix least-squares techniques minimizing $\sum w(|F_o| - |F_c|)^2$. Final refinement with anisotropic thermal parameters for non-hydrogen atoms converged to $R = 0.059$ ($R_w = 0.051$) (**8b**) and $R = 0.045$ ($R_w = 0.033$) (**15a**), respectively, where $R = \sum||F_o| - |F_c||/\sum|F_o|$ and $R_w = [\sum w(|F_o| - |F_c|)^2/\sum w|F_o|^2]^{1/2}$ ($w = 1/\sigma^2(F_o)$). Atomic scattering factors and values of f' and f'' for Pt, Cl, P, F, N, and C were taken from refs 18 and 19. All calculations were carried out on a Digital VAX Station 3100 M38 with the TEXSAN-TEXRAY Program System. The perspective views were drawn by using the program ORTEP.[20]

Compounds 11a and 13a. The coordinates of the two platinum atoms were determined from Patterson vectors, and subsequent Fourier syntheses gave the positions of other non-hydrogen atoms. The coordinates of all hydrogen atoms except for those of the solvent molecules were calculated at ideal positions with a C–H distance of 0.95 Å. The structure was refined with full-matrix least-squares techniques. Final refinement with anisotropic thermal parameters for non-hydrogen atoms (hydrogen atoms were not refined) converged to $R = 0.048$ and $R_w = 0.046$ ($w = 1/\sigma^2(F_o)$) for **13a** and $R = 0.054$ and $R_w = 0.040$ for **11a**.

Compound 14a. The structure was solved by direct methods with MULTAN78[21] and UNICS III.[22] The three platinum atoms were located in the initial E map, and subsequent Fourier syntheses gave the positions of other non-hydrogen atoms. The coordinates of all hydrogen atoms were calculated at ideal positions with a C–H distance of 0.95 Å and were not refined. The structure was refined with full-matrix least-squares techniques. Final refinement with anisotropic thermal parameters for the Pt, P, and F atoms and with isotropic temperature factors for the other non-hydrogen atoms converged to $R = 0.056$ and $R_w = 0.038$ ($w = 1/\sigma^2(F_o)$). The absolute configuration was not determined, and f'' values were not included in F_c.

Compound 16a. The structure was solved by direct methods with MITHRIL. The platinum atoms were located in the initial E map, and subsequent Fourier syntheses gave the positions of other non-hydrogen atoms. The coordinates of the H(1) atom were determined by difference Fourier synthesis using reflections with $2\theta < 40°$, and those of the other hydrogen atoms were calculated at ideal positions with a C–H distance of 0.95 Å. The structure was refined with full-matrix least-squares techniques. Final refinement with anistropic thermal parameters for non-hydrogen atoms (hydrogen atoms were not refined) converged to $R = 0.044$ and $R_w = 0.035$ ($w = 1/\sigma^2(F_o)$).

X-ray Absorption Analysis. X-ray absorption measurements around the Pt L_3 edge (10.856–13.056 keV) were performed at the Photon Factory of the National Laboratory for High Energy Physics[23] on beam line 10B using synchrotron radiation (2.5 GeV, 340–300 mA). The experiments were done in the transmission mode on powdered samples using a Si(311) monochromator. The theoretical expression of the obtained $k^3\chi(k)$ for the case of single scattering is[24]

$$\mathbf{k}^3\chi(\mathbf{k}) = \sum_i[(\mathbf{k}^2N_i/N_i/r_i^2)S_iF_i(\mathbf{k})\exp(-2\sigma_i^2\mathbf{k}^2) \times \sin(2\mathbf{k}r_i+\Phi_i(\mathbf{k}))]$$

where r_i, N_i, S_i, $F_i(k)$, $\Phi_i(k)$, and σ_i represent the interatomic distance, the coordination number, the reducing factor, the backscattering amplitude, the phase shift, and the Debye–Waller factor, respectively, and $\mathbf{k}$ is the photoelectron wave vector defined as $\mathbf{k} = [(2m/\hbar^2)(E-E_0)]^{1/2}$ ($E_0 = 11.562$ keV). The backscattering amplitude $F_i(\mathbf{k})$ and the phase shift $\Phi_i(\mathbf{k})$ functions employed were the empirical parameters derived from the analysis of **8b**,[25] and N_i and r_i were varied in the nonlinear least-squares refined curve fitting with σ_i fixed to 0.06 Å (the theoretical parameters tabulated by Teo and Lee were used in the preliminary analyses).[26] All calculations were performed on a HITAC s-800 computer at the Computer Center of the University of Tokyo with the systematic programs EXAFS1.[27]

Molecular Orbital Calculations. Extended Hückel molecular orbital calculations were carried out by using parameters of the Coulomb integrals and the orbital exponents taken from ref 28. For the Pt d functions, a double-ζ expansion was used. Geometrical assumptions were derived from the crystal structure **14a**: Pt–Pt = 2.64 Å, Pt–P = 2.30 Å, Pt–C = 1.97 Å, N–C = 1.15 Å, P–H = 1.42 Å, and N–H = 1.01 Å.

Results and Discussion

Preparation of $[Pt(diphos)(RNC)_2](PF_6)_2$ (diphos = dppen (1), dppe (2), dppp (3), dppb (4), and dtbpe (5)). The reaction of $PtCl_2(COD)$ (1 equiv) with diphosphines (diphos = dppen, dppe, dppp, or dppb) (1 equiv) and aromatic isocyanides (RNC) (2 equiv) in the presence of an excess of NH_4PF_6 gave colorless to pale yellow complexes formulated as $[Pt(diphos)(RNC)_2](PF_6)_2$ (**1a**, diphos = dppen, R = 2,6-$Me_2C_6H_3$ (Xyl); **1b**, diphos = dppen, R = 2,4,6-$Me_3C_6H_2$ (Mes); **2a**, diphos = dppe, R = Xyl; **2b**, diphos = dppe, R = Mes; **3a**, diphos = dppp, R = Xyl; **3b**, diphos = dppp, R = Mes; **4a**, diphos = dppb, R = Xyl; **4b**, diphos = dppb, R = Mes) in good yields (64–99%). Two IR absorptions corresponding to *sym*- and *asym*-stretching vibrations of the N≡C groups are expected in compounds 1–4, tentatively having *cis* geometry of RNC, but the IR spectra of 1–4 showed only one peak at 2209–2232 cm^{-1} corresponding to the terminal isocyanide groups ($\nu_{N\equiv C}$), probably due to an accidental degeneracy. The ^1H NMR spectra indicated the presence of one kind of isocyanide and diphosphine ligands, and the electronic absorption spectra were similar to that of $[Pt(RNC)_4](PF_6)_2$,[8] suggesting a square planar coordination geometry. Similarly, the reaction of $PtCl_2$(dtbpe) with RNC and NH_4PF_6 gave $[Pt(dtbpe)(RNC)_2](PF_6)_2$ (**5a**, R = Xyl, 97%; **5b**, R = Mes, 77%). The IR spectra of **5** showed two peaks around 2200 cm^{-1}, corresponding to *sym*- and *asym*-stretching vibrations of the N≡C groups in a *cis* arrangement. In the ^1H NMR spectra, only one resonance for the ^{t}Bu groups was observed at $\delta \sim 1.6$ as

(16) The X-ray crystallographic analysis of **11a** described in our preliminary report was revised by using another suitable crystal in this work, and that of **14a** was also revised with full-matrix least squares refinement.

(17) Gilmore, G. J. *J. Appl. Crystallogr.* **1984**, *17*, 42.
(18) Cromer, D. T.; Waber, J. T. *International Tables for X-ray Crystallography*; Kynoch Press: Birmingham, England, 1974; Vol. IV.
(19) Cromer, D. T. *Acta Crystallogr.* **1965**, *18*, 17.
(20) Johnson, C. K. *ORTEP-II, a FORTRAN Thermal Ellipsoid Plot Program*; Oak Ridge National Laboratory: Oak Ridge, TN, 1976.
(21) Main, P.; Lessinger, L.; Woolfson, M. M.; Germain, G.; Declerq, J. P. *MULTAN78*; Universities of York and Louvain: York, England, and Louvain, Belgium, 1978.
(22) Sakurai, T.; Kobayashi, K. *Rikagaku Kenkyusho Hokoku* **1979**, *55*, 69.
(23) *Photon Factory Activity Report*; National Laboratory for High Energy Physics: Ibaraki, Japan, 1986; No. 3.
(24) Sayers, D. E.; Stern, E. A.; Lytle, F. W. *Phys. Rev. Lett.* **1971**, *27*, 1204.
(25) Cramer, S. P.; Hodgson, K. O.; Gillum, W. O.; Mortenson, L. E. *J. Am. Chem. Soc.* **1978**, *100*, 3398.
(26) (a) Teo, B. K.; Lee, P. A.; Simons, A. L.; Eisenberger, P.; Kincaid, B. M. *J. Am. Chem. Soc.* **1977**, *99*, 3854. (b) Teo, B. K.; Lee, P. A. *J. Am. Chem. Soc.* **1979**, *101*, 2815.
(27) Kosugi, N.; Kuroda, H. *Program EXAFS1*; Research Center for Spectrochemistry, the University of Tokyo: Tokyo, Japan, 1985.
(28) Dedieur, A.; Hoffmann, R. *J. Am. Chem. Soc.* **1978**, *100*, 2074.

Table 2. Reduction Peak Potentials of [Pt(diphos)(RNC)$_2$](PF$_6$)$_2$[a]

complex	E^1_{pc}, V[b]	E^2_{pc}, V[b]
[Pt(dppen)(XylNC)$_2$]$^{2+}$ (**1a**)	−1.12	−1.63
[Pt(dppen)(MesNC)$_2$]$^{2+}$ (**1b**)	−1.16	−1.65
[Pt(dppe)(XylNC)$_2$]$^{2+}$ (**2a**)	−1.23	−1.82
[Pt(dppe)(MesNC)$_2$]$^{2+}$ (**2b**)	−1.28	−1.84
[Pt(dppp)(XylNC)$_2$]$^{2+}$ (**3a**)	−1.30	−1.78
[Pt(dppp)(MesNC)$_2$]$^{2+}$ (**3b**)	−1.34	−1.81
[Pt(dppb)(XylNC)$_2$]$^{2+}$ (**4a**)	−1.23	*c*
[Pt(dppb)(MesNC)$_2$]$^{2+}$ (**4b**)	*d*	*d*
[Pt(dtbpe)(XylNC)$_2$]$^{2+}$ (**5a**)	−1.35	−1.94
[Pt(dtbpe)(MesNC)$_2$]$^{2+}$ (**5b**)	−1.40	−1.96

[a] Cyclic voltammograms were measured on 0.5–1.0 mM solutions of the complexes in acetonitrile containing 0.1 M [^{n}Bu$_4$N][ClO$_4$] by means of a platinum-button electrode (1.6-mm i.d.) with a scanning rate of 200 mV/s. [b] Referenced to the $E_{1/2}$ of the redox coupling, Cp_2Fe/Cp_2Fe^+ (1.0 mM in CH_3CN). [c] Not observed. [d] Could not be measured due to its insolubility.

a doublet (J_{PH} ~ 16 Hz) and one peak for the *o*-methyl groups of isocyanides at δ ~ 2.5 as a singlet.

Cyclic voltammograms (CV) of complexes **1**–**5** in an acetonitrile solution containing 0.1 M [^{n}Bu$_4$N][ClO$_4$] were measured to investigate the conditions of controlled-potential reductions (Table 2). The CV of **2a** showed two irreversible reduction waves at −1.22 V (E^1_{pc}) and −1.82 V (E^2_{pc}). By analogy with [Pt(PPh$_3$)$_2$(XylNC)$_2$](PF$_6$)$_2$ and [Pt(dppm)(XylNC)$_2$](PF$_6$)$_2$,[8] they corresponded to two-step one-electron reductions, Pt(II) → Pt(I) and Pt(I) → Pt(0). The CVs of **1**, **2b**, **3**, and **5** also showed two irreversible reduction waves at −1.12 to −1.40 V (E^1_{pc}) and −1.55 to −1.96 V (E^2_{pc}). The peak potentials of E^1_{pc} and E^2_{pc} for compounds **5** are lower than those for **1**–**3**, because of the high electron-donating ability of dtbpe. In contrast, the CV of **4a** showed only one irreversible reduction wave at −1.23 V, similar to that of PtCl$_2$(XylNC)$_2$, seemingly corresponding to a one-step two-electron transfer, Pt(II) → Pt(0).[6a]

Electrochemical Preparation of [Pt$_2$(diphos)$_2$(RNC)$_2$](PF$_6$)$_2$ (diphos = dppen (6), dppe (7), dppp (8), and dppb (9)). The controlled potential electrolyses of **1**–**4** in acetonitrile containing 0.1 M NaClO$_4$ at a mercury-pool electrode were carried out at −1.45 to −1.5 V (**1**–**4**) (lower potential than E^1_{pc}) and consumed ca. 1 F mol^{-1} of the starting complexes to afford pale yellow to yellow dinuclear complexes, [Pt$_2$(diphos)$_2$(RNC)$_2$](PF$_6$)$_2$ (**6a**, diphos = dppen, R = Xyl; **6b**, diphos = dppen, R = Mes; **7a**, diphos = dppe, R = Xyl; **7b**, diphos = dppe, R = Mes; **8a**, diphos = dppp, R = Xyl; **8b**, diphos = dppp, R = Mes; **9a**, diphos = dppb, R = Xyl; **9b**, diphos = dppb, R = Mes). The electrochemical formation of diplatinum compounds **1**–**3** is assumed to proceed via an initial one-electron reduction of Pt(II) to Pt(I) and a subsequent dimerization process, and in the case of **4** via an initial two-electron reduction of Pt(II) to Pt(0) and a concomitant conproportionation, Pt(0) + Pt(II) → 2Pt(I). Complexes **6**–**8** could also be prepared by the electrochemical reduction of the monomers (**1**–**3**) at −1.8 V (lower potential than E^2_{pc}), with yields being suppressed owing to the formation of further reduced species. These reactions may also proceed via a two-electron reduction of Pt(II) and a subsequent conproportionation as in the case of **4**.

The IR spectra of **6**–**9** show a sharp peak at 2143–2171 cm^{-1}, corresponding to the terminal isocyanide groups. The $\nu_{N\equiv C}$ frequencies shifted to lower energy by ca. 70 cm^{-1} than those of the starting compounds **1**–**4**, indicating that the divalent platinum center was reduced to a monovalent species. In the UV–vis spectra, the lowest energy absorption band at 285–317 nm was assigned to the σ–σ^* transition of a Pt–Pt bond by analogy to [Pt$_2$(PPh$_3$)$_2$(XylNC)$_4$]$^{2+}$ (303 nm) and [Pt$_2$(dppm)$_2$(XylNC)$_2$]$^{2+}$ (292 nm),[8] and this assignment was further substantiated by the fact that the photolysis of a mixture of **8b** (0.03 mM) and CCl_4 (0.15 mM) in CH_3CN cleaved the metal–metal bond to give [PtCl(dppp)(MesNC)](PF$_6$).[29] It is known that photoexcitation of [Pt$^I_2$L$_6$]$^{2+}$ complexes in CX_4 affords [Pt^{II}XL$_3$]$^+$ species.[30] The ^{1}H NMR spectra indicated the presence of one type of isocyanide ligand, and the ^{31}P{^{1}H} NMR spectra showed two sets of resonances in the region −10 to 90 ppm, indicating that each end of the diphosphine ligand is in a chemically distinct environment. The ^{31}P{^{1}H} NMR spectrum of **6a** showed two sets of resonances centered at δ 60.0 and 84.0, both of which are accompanied by complex satellite peaks due to coupling to ^{195}Pt (I = $^1/_2$). The observed spectrum is explicable in a combination of three isotopomers, P$_2$Pt–PtP$_2$, P$_2$Pt–^{195}PtP$_2$, and P$_2$^{195}Pt–^{195}PtP$_2$ (their ratios calculated from the natural abundance are 4:4:1). From the lower field set (A) centered at δ 84.0, the values of $^1J_{PPt}$, $^2J_{PPt}$, and $^3J_{PP}$ were assumed to be 2065, 461, and 150 Hz, respectively, which were similar to those of [Pt$_2$(PPh$_3$)$_2$(XylNC)$_4$](PF$_6$)$_2$.[31] These indicate that resonance A corresponds to the phosphorus atoms occupying the position *trans* to the Pt–Pt bond. From the higher field set (B) centered at δ 60.0, $^1J_{P'Pt}$ and $^2J_{P'Pt}$ were estimated to be 3091 and −38 Hz, and $^3J_{P'P'}$ was not observed; these were reminiscent of the dppm-bridged dimers[32] and indicated that resonance B corresponds to the phosphorus atoms in the *cis* position to the Pt–Pt bond. The small coupling constant of $J_{PP'}$ (9.0 Hz) is indicative of a *cis* orientation of the two dissimilar phosphorus atoms.[10,33] The ^{31}P{^{1}H} NMR spectra of **7a**, **8a**, and **8b** also showed similar patterns (Table 3). These spectral data suggested that complexes **1**–**4** have a dinuclear structure with a Pt(I)–Pt(I) σ-bond, where the diphosphine ligands chelate to a Pt atom. The dimers with bridging diphosphines were not obtained in the present reactions, tentatively due to the instability of large-membered metal-containing macrocyclic conformations. The complexes **6**–**8** could also be prepared by the substitution reaction of Pt$_2$Cl$_2$(RNC)$_4$ (R = Xyl, Mes) with 2 equiv of diphosphines (dppen, dppe, dppp, and dppb) in the presence of an excess amount of NH$_4$PF$_6$ in good yields.

An X-ray crystallographic study of **8b** was undertaken. A perspective drawing of the complex cation of **8b** with the atomic numbering scheme is given in Figure 1. Some selected bond distances and angles are listed in Table 4. The complex cation consists of two platinum atoms joined by a platinum–platinum σ-bond. Each platinum atom is

(29) An acetonitrile solution containing 0.03 mM **8b** and 0.15 mM carbon tetrachloride was irradiated for 2 h by a Rikokagaku UVL-100P 100-W high-pressure mercury lamp through a water IR filter. The solvent was removed under reduced pressure; the residue was extracted with CH_2Cl_2 (30 mL) and concentrated to 10 mL; and addition of Et_2O gave pale yellow crystals of [PtCl(dppp)(MesNC)](PF$_6$). Yield: 46%. Anal. Calcd for $C_{37}H_{37}NPtClP_3F_6$: C, 47.62; H, 4.00; N, 1.50. Found: C, 47.53; H, 3.97; N, 1.72. IR (Nujol): $\nu_{N\equiv C}$ 2200 cm^{-1}. UV–vis (CH_3CN): λ_{max} 255 nm. The photochemical reactions of di- and triplatinum complexes will be reported elsewhere.

(30) Reinking, M. K.; Kullberg, M. L.; Cutler, A. R.; Kubiak, C. P. *J. Am. Chem. Soc.* **1985**, *107*, 3517.

(31) Briant, C.; Gilmour, D. I.; Mingos, D. M. P. *J. Organomet. Chem.* **1986**, *308*, 381.

(32) Brown, M. P.; Puddephatt, R. J.; Rashidi, M.; Seddon, K. R. *J. Chem. Soc., Dalton Trans.* **1977**, 951.

(33) Lindsay, C. H.; Benner, L. S.; Balch, A. L. *Inorg. Chem.* **1980**, *19*, 3503.

Table 3. $^{31}P\{^1H\}$ NMR Spectral Data of $[Pt_2(diphos)_2(RNC)_2]^{2+}$, $[\{Pt(diphos)(RNC)\}_2Pt(RNC)_2]^{2+}$, and $[\{Pt(diphos)(RNC)\}_2Pt]^{2+}$

(A) P—Pt(P')—Pt—P (B) P—Pt(P')—Pt—Pt(P')—P

complexes[a]	δ_P, ppm	$\delta_{P'}$, ppm	$^1J_{PPt}$, Hz	$^1J_{P'Pt}$, Hz	$^2J_{PPt}$, Hz	$^2J_{P'Pt}$, Hz	$^3J_{PPt}$, Hz	$^3J_{P'Pt}$, Hz	$^2J_{PP'}$, Hz	$^{3or4}J_{PP}$, Hz
$[Pt_2(dppen)_2(XylNC)_2]^{2+}$ (**6a**)[b]	84.0	60.0	2065	3091	461	−38			9	150
$[Pt_2(dppe)_2(XylNC)_2]^{2+}$ (**7a**)[b]	63.3	48.3	2023	3119	434	−34			6	142
$[Pt_2(dppp)_2(XylNC)_2]^{2+}$ (**8a**)[b]	−2.4	−4.5	2019	3092	355	*d*			30	135
$[Pt_2(dppp)_2(MesNC)_2]^{2+}$ (**8b**)[b]	−2.5	−4.4	2018	3100	358	*d*			30	136
$[Pt_3(dppe)_2(XylNC)_4]^{2+}$ (**10a**)[c]	78.5	51.8	2058	3314	559	58	26	*d*	12	46
$[Pt_3(dppen)_2(XylNC)_4]^{2+}$ (**11a**)[c]	94.6	61.0	2064	3327	570	63	31	18	10	51
$[Pt_3(dppen)_2(XylNC)_2]^{2+}$ (**13a**)[c]	92.6	62.5	2157	3090	1632	218	286	29	10	100
$[Pt_3(dtbpe)_2(XylNC)_2]^{2+}$ (**15a**)[c]	126.7	102.0	2081	3126	1505	117	273	12	5	89

[a] Measured at 63.32 MHz in CD_2Cl_2 at room temperature. [b] See structure **A**. [c] See structure **B**. [d] Not resolved.

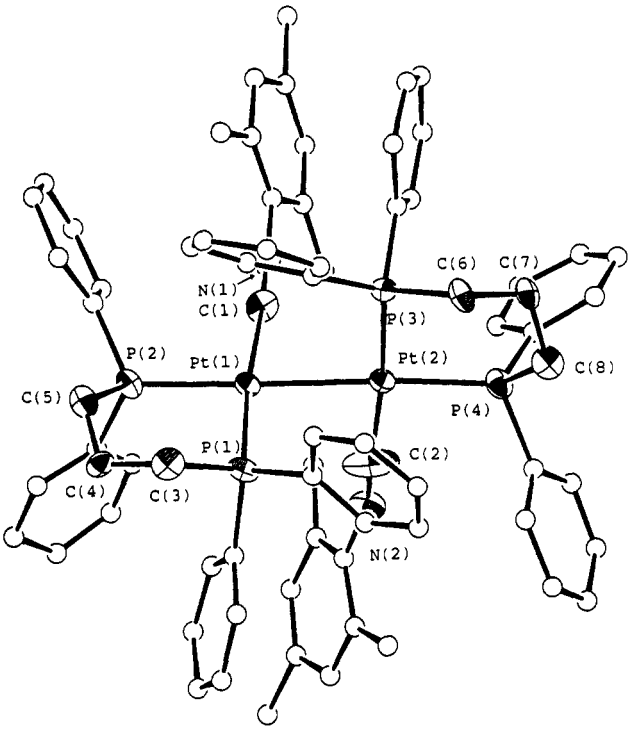

Figure 1. A perspective drawing of the complex cation of **8b**, $[Pt_2(dppp)_2(MesNC)_2]^{2+}$.

coordinated by two phosphorus atoms of bidentate dppp ligand, a terminal carbon atom of isocyanide, and another platinum atom in a nearly planar array. The structure of **8b** is isomorphous to that of the palladium analogue, $[Pd_2(dppp)_2(MesNC)_2](PF_6)_2$ (**18**).[10] The dihedral angle between the two $[PtP_2C]$ coordination planes is 85°, nearly perpendicular as observed in **18** (86°). A dihedral angle of 90° is ideal for minimizing the repulsion between the ligands, and an angle of 45° ideal is for minimizing repulsive overlap of the out-of-plane metal dπ orbitals on adjacent metal centers.[34] In the nonbridged dimer **8b**, the steric factor seems to be responsible for the observed structure.

The Pt–Pt bond length of 2.653(1) Å is significantly longer than that of the unbridged platinum(I) isocyanide dimer, $Pt_2Cl_2(2,4\text{-}^tBu_2\text{-}6\text{-}MeC_6H_2NC)_4$ (2.562 Å),[6b] longer by 0.036 Å than is found in the Pd analogue **18** (2.617(2) Å), and is comparable to that found in dppm-bridged dimers, $Pt_2Cl_2(\mu\text{-dppm})_2$ (2.652 Å).[35] The axial P atoms are collinear with the Pt–Pt bond, and the average Pt–

Table 4. Selected Bond Distances (Å) and Angles (deg) of 8b[a]

Bond Distances			
Pt(1)–Pt(2)	2.653(1)		
Pt(1)–P(1)	2.287(5)	Pt(1)–P(2)	2.326(5)
Pt(2)–P(3)	2.327(5)	Pt(2)–P(4)	2.298(6)
Pt(1)–C(1)	1.95(2)	Pt(2)–C(2)	2.03(2)
P(1)–C(3)	1.83(2)	P(2)–C(5)	1.83(2)
P(3)–C(6)	1.89(2)	P(4)–C(8)	1.84(2)
N(1)–C(1)	1.16(2)	N(1)–C(11)	1.42(2)
N(2)–C(2)	1.11(2)	N(2)–C(21)	1.41(2)
C(3)–C(4)	1.49(2)	C(4)–C(5)	1.45(2)
C(6)–C(7)	1.46(2)	C(7)–C(8)	1.53(2)
Bond Angles			
Pt(2)–Pt(1)–P(1)	89.3(1)	Pt(2)–Pt(1)–P(2)	176.5(1)
Pt(2)–Pt(1)–C(1)	83.7(5)	P(1)–Pt(1)–P(2)	94.1(2)
P(1)–Pt(1)–C(1)	171.7(6)	P(2)–Pt(1)–C(1)	92.9(6)
Pt(1)–Pt(2)–P(3)	95.8(1)	Pt(1)–Pt(2)–P(4)	169.1(1)
Pt(1)–Pt(2)–C(2)	79.3(8)	P(3)–Pt(2)–P(4)	93.4(2)
P(3)–Pt(2)–C(2)	173.9(7)	P(4)–Pt(2)–C(2)	91.8(8)
C(1)–N(1)–C(11)	176(2)	C(2)–N(2)–C(21)	166(3)
Pt(1)–C(1)–N(1)	176(2)	Pt(2)–C(2)–N(2)	176(2)

[a] Estimated standard deviations in parentheses.

Pt–P_{ax} angle is 172.8°. The six-membered chelate rings adopt a chair conformation, and the average bite angle is 93.8°. There is no short contact (<3.3 Å) between the phenyl rings on the equatorial phosphorus atom and the neighboring platinum atom. Each isocyanide ligand is bent toward another Pt atom. The Pt(2)–Pt(1)–C(1) and Pt(1)–Pt(2)–C(2) are 83.7(5)° and 79.3(8)°, the latter bringing the Pt(1)···C(2) distance to 3.03(3) Å. The inward bend of the equatorial isocyanides is largely attributable to the steric bulk of dppp ligands. It is caused in part by an electronic effect arising from interaction between the filled d orbitals of the platinum with the empty π^* orbitals of the isocyanide ligands on the adjacent metal.[36]

In order to examine the length of the platinum–platinum bond of other binuclear complexes, EXAFS (extended X-ray absorption fine structure) analyses were performed on **6a**, **7a**, **8a**, **8b**, and **9a**. The Fourier transform of these compounds showed three peaks in the range of 1.1–2.7 Å (before phase-shift correction); the small peak at ca. 1.6 Å is assigned to the back-scattering contribution of the terminal carbon atom of isocyanide, the intense peak at ca. 1.9 Å corresponds to that of the phosphorus atoms of the diphosphine ligands, and the peak at about 2.5 Å is attributable to the platinum atom. These peaks were back Fourier transformed by the use of a proper window and

(34) Kullberg, M. L.; Lemke, F. R.; Powell, D. R.; Kubiak, C. P. *Inorg. Chem.* **1985**, *24*, 3589.

(35) Manojlovic-Muir, Lj.; Muir, K. M.; Salomun, T. *Acta Crystallogr.* **1979**, *B35*, 1237.

(36) Goldberg, S. Z.; Eisenberg, R. *Inorg. Chem.* **1976**, *15*, 535.

Table 5. Distances of Pt–Pt Bonds Derived from EXAFS Analyses

complex	EXAFS r, Å[a]	EXAFS N[b]	crystallogr r, Å[c]
$[Pt_2(dppen)_2(XylNC)_2]^{2+}$ (**6a**)	2.653	1.1	
$[Pt_2(dppe)_2(XylNC)_2]^{2+}$ (**7a**)	2.635	1.1	
$[Pt_2(dppp)_2(XylNC)_2]^{2+}$ (**8a**)	2.648	0.9	
$[Pt_2(dppp)_2(MesNC)_2]^{2+}$ (**8b**)	*d*	*d*	2.653
$[Pt_2(dppb)_2(XylNC)_2]^{2+}$ (**9a**)	2.625	0.6	
$[Pt_3(dppe)_2(XylNC)_4]^{2+}$ (**10a**)	2.651	1.1	
$[Pt_3(dppen)_2(XylNC)_4]^{2+}$ (**11a**)	2.650	1.3	2.655
$[Pt_3(dtbpe)_2(XylNC)_4]^{2+}$ (**12a**)	2.664	0.7	
$[Pt_3(dppen)_2(XXylNC)_2]^{2+}$ (**13a**)	2.633	1.1	2.615
$[Pt_3(dppp)_2(XylNC)_2]^{2+}$ (**14a**)	2.647	0.9	2.640[e]
$[Pt_3(dtbpe)_2(XylNC)_2]^{2+}$ (**15a**)	2.648	1.0	2.6409
$[Pt_3(PPh_3)_2(XylNC)_6]^{2+}$ (**19**)	2.632	1.6	2.6389[f]

[a] The Pt–Pt lengths determined by EXAFS analyses; estimated errors are ±0.008 Å. [b] The number of neighboring platinum atoms; estimated errors are ±0.3. [c] The Pt–Pt bond distances determined by X-ray crystallographic analyses. [d] Reference compound. The values determined by X-ray crystallography were used to determine the parameters of $F_{Pt}(k)$ and $\Phi_{Pt}(k)$. [e] Average value. [f] Reference 7.

were subjected to curve-fitting analyses using empirical parameters derived from **8b**. The structural parameters are summarized in Table 5. In the series of bis(diphosphine) dimers, the Pt–Pt bond lengths fall in a narrow range (2.625–2.653 Å) and are hardly influenced by the methylene chains of diphosphines.

The controlled-potential electrolysis of $[Pt(dtbpe)(RNC)_2](PF_6)_2$ (**5**) at −1.45 V (consumed 1 F mol^{-1}) and the chemical reaction of $[Pt_2(RNC)_6](PF_6)_2$ with 2 equiv of dtbpe did not give a dimeric complex involving a Pt–Pt bond. These failures imply the highly unstable property of the Pt–Pt bond in $[Pt_2(dtbpe)_2(RNC)_2]^{2+}$, presumably due to steric repulsion between adjacent bulky dtbpe ligands.

Electrochemical and Chemical Preparations of $[\{Pt(diphos)(RNC)\}_2Pt(RNC)_2](PF_6)_2$ (diphos = dppe (10), dppen (11), and dtbpe (12)). The controlled-potential electrolysis of $[Pt(dppe)(RNC)_2](PF_6)_2$ (**2**) consumed 1.5 F mol^{-1} of the complex at −1.8 V (lower potential than E^2_{pc} of **2**), and the subsequent workup gave red-orange crystals of $[\{Pt(dppe)(RNC)\}_2Pt(RNC)_2](PF_6)_2 \cdot n CH_2Cl_2$ (**10a**, R = Xyl, n = 0.5, 70%; **10b**, R = Mes, n = 2, 19%), whereas a similar electroreduction at −1.45 V (between E^1_{pc} and E^2_{pc}) afforded the dinuclear complex **7** as a main product. The analogous complex, $[\{Pt(dppen)(RNC)\}_2Pt(RNC)_2](PF_6)_2$ (**11a**, R = Xyl; **11b**, R = Mes), as well as **10** was readily prepared by the ligand substitution reaction of the linear triplatinum complex of isocyanides, $[Pt_3(RNC)_8]^{2+}$,[7,8] with 2 equiv of diphosphine (dppe or dppen) in dichloromethane at room temperature. Treatment of the dimers **6a** and **7a** with $Pt^0_3(XylNC)_6$ in refluxing acetonitrile also gave the trimers **10a** and **11a**. Although the yields were not so good (10–14%), these might suggest that the mechanism for formation of the trimer $[\{Pt(diphos)(RNC)\}_2Pt(RNC)_2]^{2+}$ in the electrolysis involves a reaction of the dimer $[Pt_2(diphos)_2(RNC)_2]^{2+}$ with a zerovalent platinum species, presumably a d^{10} $Pt(RNC)_2$ fragment. A similar insertion reaction of a d^{10} $Pt(RNC)_2$ fragment into a Pt–Pt bond of $[Pt_2(dppm)_2(RNC)_2]^{2+}$ has been described.[7,8]

In the electronic absorption spectra, the lowest energy absorption was observed at 403–408 nm, which was red-shifted by ca. 90 nm compared with those of the corresponding dimers **6** and **7** (Figure 2a). Further, the similarity of the spectral pattern to that of $[Pt_3(PPh_3)_2(XylNC)_6](PF_6)_2$ (**19**)[7,8,31] suggested a linear triplatinum structure with two phosphorus atoms in the axial positions. The IR and ^1H NMR spectra of **10** and **11** indicated the presence of two kinds of terminal isocyanide ligands. The $^{31}P\{^1H\}$ NMR spectra of **10a** and **11a** showed two sets of complicated peaks centered at δ 51.8 and 78.5 (**10a**) and δ 61.0 and 94.6 (**11a**), suggesting two distinct environments of phosphorus atoms as observed in the diplatinum compounds. Both spectral patterns were identical to each other. The spectrum of **11a** is in accord with a combination of six isotopomers, P_2Pt–Pt–PtP_2, P_2Pt–Pt–$^{195}PtP_2$, P_2-Pt–^{195}Pt–PtP_2, P_2Pt–^{195}Pt–$^{195}PtP_2$, $P_2{}^{195}Pt$–Pt–$^{195}PtP_2$, and $P_2{}^{195}Pt$–^{195}Pt–$^{195}PtP_2$ with the ratio of 8:8:4:4:2:1 (Figure 3a). The lower field set was assigned to the P atoms in the *trans* position to the Pt–Pt bonds from the large *trans* couplings of $^2J_{PPt}$ = 570 Hz, $^3J_{PPt}$ = 31 Hz, and $^4J_{PP}$ = 51 Hz, and the higher field set was assigned to those in the *cis* position to the Pt–Pt bonds from the large $^1J_{P'Pt}$ (3327 Hz) and the absence of $^4J_{P'P'}$ coupling, which were similar to those in **6a** (Table 3).

An X-ray crystallographic study of **11a** was performed to confirm the detailed structure of the triplatinum complexes. The unit cell contains two discrete complex cations, four hexafluorophosphate anions, and four solvent molecules, with no unusual contact between the fragments. A perspective drawing of the complex cation of **11a** with the atomic numbering scheme is given in Figure 4, and selected bond lengths and angles are listed in Table 6. The cation possesses a crystallographically imposed inversion center and consists of three platinum atoms in a linear arrangement, the Pt–Pt–Pt angle being constrained to 180°. Each Pt atom exhibits approximate square-planar geometry; the outer platinum (Pt(2)) is coordinated by two P atoms of chelating dppen ligand, one terminal isocyanide, and a neighboring Pt atom, and the central platinum atom (Pt(1)) is coordinated by two terminal isocyanides and two Pt atoms. The square planes are nearly perpendicular to each other with a dihedral angle of 84° to minimize the steric repulsion between the ligands on adjacent Pt atoms. The whole structure is analogous to those of $[Pt_3(PPh_3)_2(XylNC)_6](PF_6)_2$ (**19**)[7,8,31] and $[Pt_3(PPh_3)_2(MeNC)_6](PF_6)_2$ (**20**).[37] The Pt–Pt bond length of 2.655(1) Å is longer than that found in **19** (2.6389(7) Å), which is ascribed to the bulky dppen ligand, in particular, the phenyl groups on the equatorial phosphorus ligands. The two axial P atoms are collinear with the three-platinum aggregate (the Pt–Pt–P_{ax} angle is 176.2(2)°). The bond length between the axial P and Pt atoms (Pt(2)–P(1) = 2.273(6)) is slightly longer than that between the equatorial P and Pt atoms (Pt(2)–P(2) = 2.248(6) Å), reflecting the high *trans* effect of Pt–Pt bonds. The five-membered chelate ring takes an envelope conformation (^{Pt}E), and the bite angle of P(1)–Pt(2)–P(1) is 86.5(2)°, which is smaller than that of dppp in **8b** (93.8°). The Pt(1)–Pt-(2)–C(2) and Pt(2)–Pt(1)–C(1) angles are 85.1(6)° and 87.4-(5)°, and the Pt(1)···C(2) and Pt(2)···C(1) distances are 3.14(2) and 3.22(2) Å. The inward bend of the terminal isocyanides toward the central Pt atom is not as large as found in **8b** and **19**.

$[\{Pt(dtbpe)(XylNC)\}_2Pt(XylNC)_2](PF_6)_2$ (**12a**) was prepared only by the substitution reaction of $[Pt_3(XylNC)_8]^{2+}$ with dtbpe in a low yield of 15%. Compound **12a** was unstable in solution even under a nitrogen atmosphere

(37) Balch, A. L.; Boehm, J. R.; Hope, H.; Olmstead, M. M. *J. Am. Chem. Soc.* **1976**, *98*, 7431.

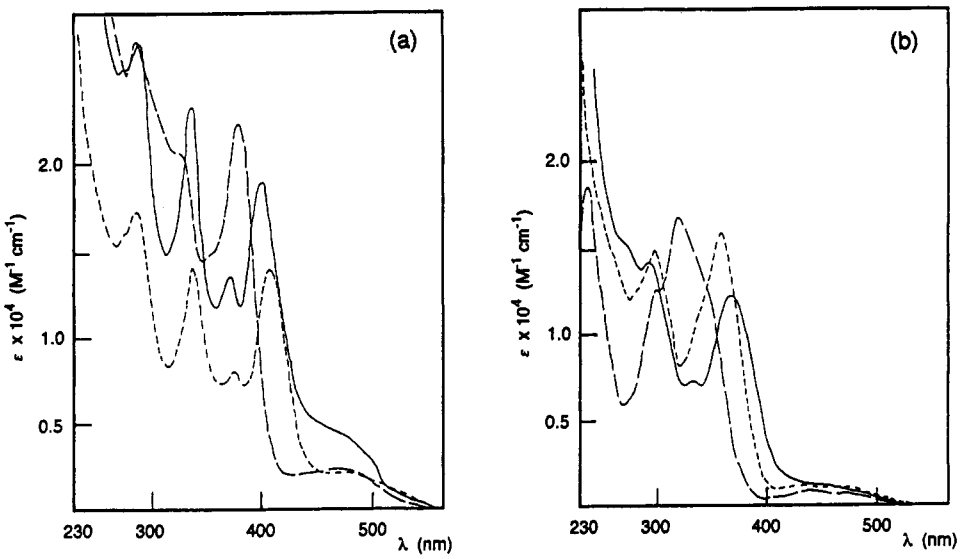

Figure 2. Electronic absorption spectra of (a) (—) $[\{Pt(dppen)(XylNC)\}_2Pt(XylNC)_2]^{2+}$ (**11a**), (- - -) $[\{Pt(dppe)(XylNC)\}_2Pt(XylNC)_2]^{2+}$ (**10a**), and (– – –) $[Pt_3(PPh_3)_2(XylNC)_6]^{2+}$ (**19**) and (b) (—) $[\{Pt(dppen)(XylNC)\}_2Pt]^{2+}$ (**13a**), (- - -) $[\{Pt(dppp)(XylNC)\}_2Pt]^{2+}$ (**14a**), and (– – –) $[\{Pt(dtbpe)(XylNC)\}_2Pt]^{2+}$ (**15a**).

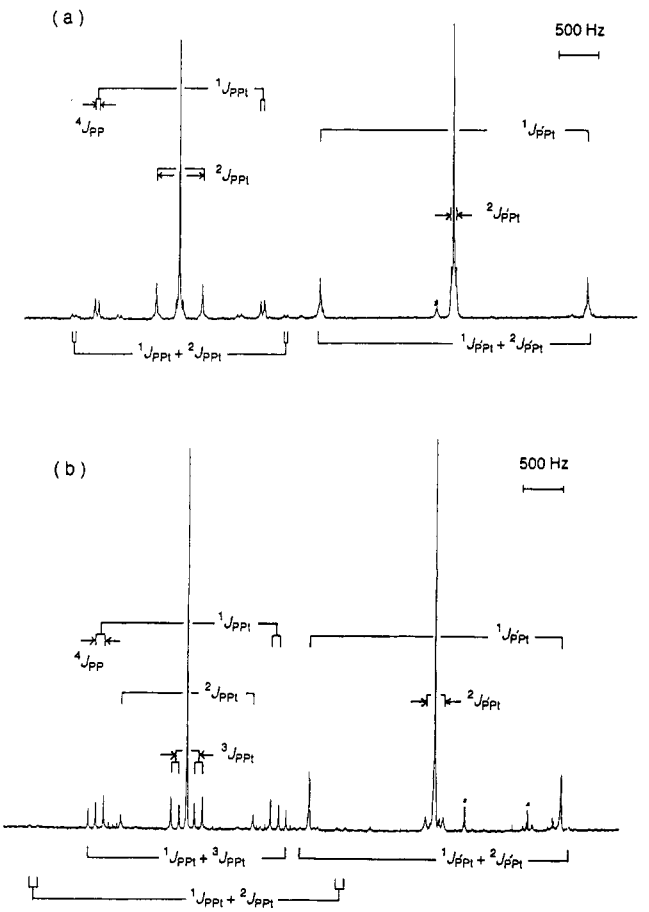

Figure 3. $^{31}P\{^1H\}$ NMR spectra of (a) $[\{Pt(dppen)(XylNC)\}_2Pt(XylNC)_2]^{2+}$ (**11a**) and (b) $[\{Pt(dppen)(XylNC)\}_2Pt]^{2+}$ (**13a**).

and readily decomposed to mononuclear species. The EXAFS analysis of **12a** indicated the average Pt–Pt bond distance to be 2.664 Å, longer than those of **10a** and **11a** (Table 5). Its instability in solution might result from an elongation of the Pt–Pt bond due to the bulky dtbpe ligands.

Electrochemical Preparation of the Coordinatively Unsaturated Triplatinum Complexes, $[\{Pt(diphos)(RNC)\}_2Pt](PF_6)_2$ (diphos = dppen (13), dppp (14), and dtbpe (15)). The controlled-potential electrolysis of $[Pt(dppen)(RNC)_2](PF_6)_2$ (1) in acetonitrile containing 0.1 M $NaClO_4$ at −1.8 V was carried out. After the passage

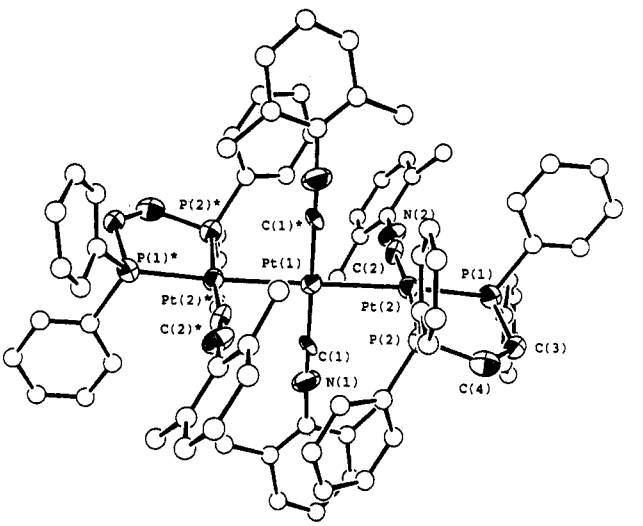

Figure 4. A perspective drawing of the complex cation of **11a**, $[\{Pt(dppen)(XylNC)\}_2Pt(XylNC)_2]^{2+}$.

Table 6. Selected Bond Distances (Å) and Angles (deg) of 11a[a]

Bond Distances			
Pt(1)–Pt(2)	2.655(1)	Pt(2)–P(1)	2.273(6)
Pt(1)–C(1)	1.94(2)	Pt(2)–C(2)	1.92(2)
Pt(2)–P(2)	2.248(6)	P(2)–C(4)	1.79(2)
P(1)–C(3)	1.82(2)	N(1)–C(1)	1.13(2)
C(3)–C(4)	1.31(2)		
N(3)–C(2)	1.19(2)		
Bond Angles			
Pt(2)–Pt(1)–Pt(2)*	180.00	Pt(2)–Pt(1)–C(1)	87.4(5)
Pt(2)–Pt(1)–C(1)*	92.6(5)	C(1)–Pt(1)–C(1)*	180.00
Pt(1)–Pt(2)–P(1)	176.2(2)	Pt(1)–Pt(2)–P(2)	91.3(2)
Pt(1)–Pt(2)–C(2)	85.1(6)	P(1)–Pt(1)–P(2)	86.5(2)
P(1)–Pt(2)–C(2)	96.8(6)	P(2)–Pt(2)–C(2)	173.4(6)
Pt(1)–C(1)–N(1)	177(2)	Pt(2)–C(2)–N(2)	169(2)
C(1)–N(1)–C(11)	176(2)	C(2)–N(2)–C(21)	177(2)
Pt(2)–P(1)–C(3)	107.0(7)	Pt(2)–P(2)–C(4)	105.4(7)
P(1)–C(3)–C(4)	115(2)	P(2)–C(4)–C(3)	124(2)

[a] Estimated standard deviations in parentheses.

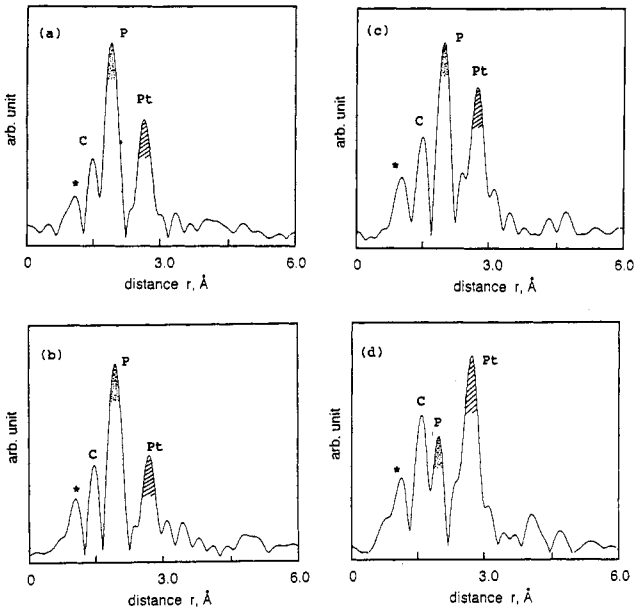

Figure 5. The Fourier transforms of EXAFS data ($k^3\chi_{obsd}(k)$) for (a) $[\{Pt(dppen)(XylNC)\}_2Pt]^{2+}$ (**13a**), (b) $[\{Pt(dppp)(XylNC)\}_2Pt]^{2+}$ (**14a**), (c) $[\{Pt(dppe)(XylNC)\}_2Pt(XylNC)_2]^{2+}$ (**10a**), and (d) $[Pt_3(PPh_3)_2(XylNC)_6]^{2+}$ (**19**).

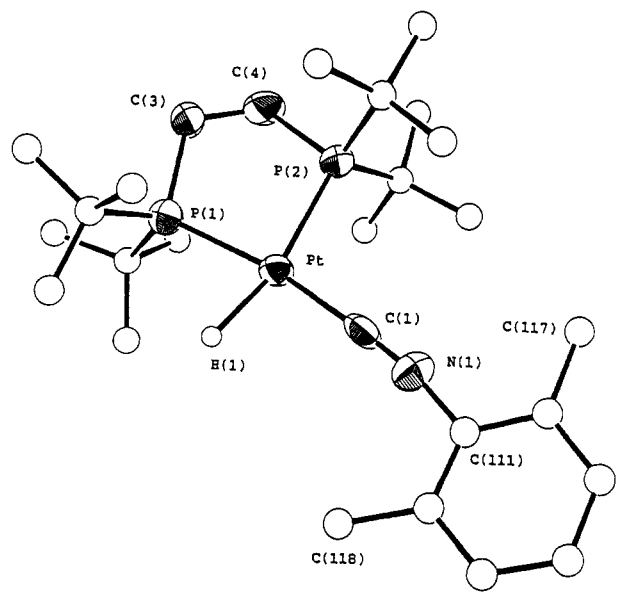

Figure 6. A perspective drawing of the complex cation of **16a**, $[PtH(dtbpe)(XylNC)]^+$. Some selected bond lengths (Å) and angles (deg): Pt(1)–P(1), 2.284(2); Pt(1)–P(2), 2.350(2); Pt–C(1), 1.947(8); Pt(1)–H(1), 1.78; N(1)–C(1), 1.174(9); P(1)–C(3), 1.832(8); P(2)–C(4), 1.847(8); C(3)–C(4), 1.53(1); P(1)–Pt(1)–P(2), 88.87(8); P(1)–Pt(1)–C(1), 168.7(2); P(2)–Pt(1)–C(1), 101.8(2); P(1)–Pt(1)–H(1), 80.3; P(2)–Pt(1)–H(1), 162.9; C(1)–Pt(1)–H(1), 88.5; Pt(1)–C(1)–N(1), 175.1(7); C(1)–N(1)–C(111), 169.5(8); Pt(1)–P(1)–C(3), 106.3(3); Pt(1)–P(2)–C(4), 105.0(3); P(1)–C(3)–C(4), 115.2(6); P(2)–C(4)–C(3), 114.0(6).

of ca. 1.5 F mol^{-1}, a mixture of $[\{Pt(dppen)(RNC)\}_2Pt](PF_6)_2 \cdot CH_2Cl_2$ (**13a**, R = Xyl, 12%; **13b**, R = Mes, 19%), the dimer **6** (8–10%), and the trimer **11** (trace) was obtained; they could be satisfactorily separated by repeated fractional recrystallizations from dichloromethane/diethyl ether. A similar electroreduction of the dppp complex **3** gave $[\{Pt(dppp)(RNC)\}_2(Pt](PF_6)_2$ (**14a**, R = Xyl, 11%; **14b**, R = Mes, 8%) together with the dimer **8** (30–40%). In the case of dtbpe, the electrolysis of **5a** at −1.8 V

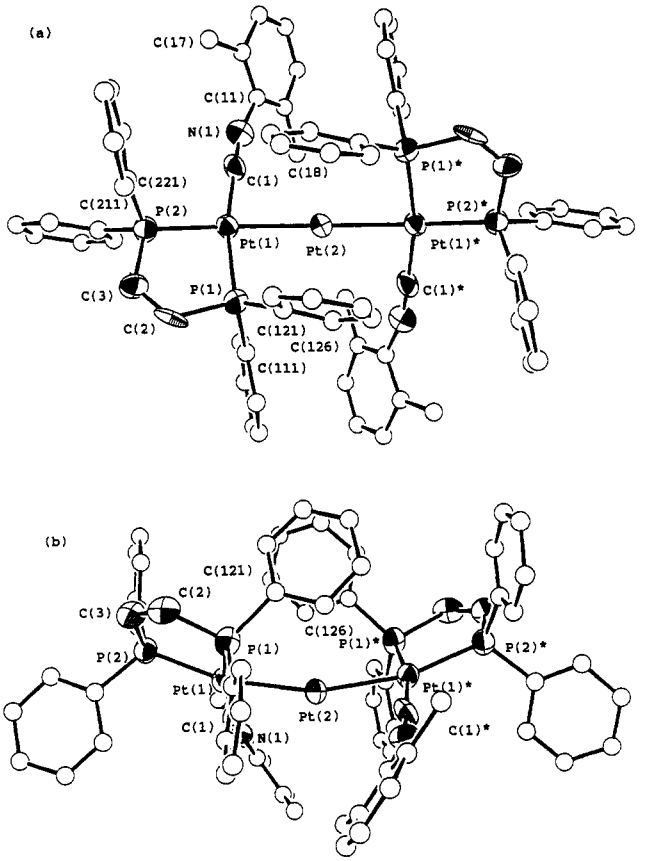

Figure 7. A perspective drawing of the complex cation of **13a**, $[\{Pt(dppen)(XylNC)\}_2Pt]^{2+}$, (a) viewed along the C_2 axis and (b) vertical to the C_2 axis.

Table 7. Selected Bond Distances (Å) and Angles (deg) of 13a[a]

Bond Distances			
Pt(1)–Pt(2)	2.615(1)	Pt(1)–P(2)	2.297(5)
Pt(1)–P(1)	2.260(5)	P(1)–C(2)	1.88(2)
Pt(1)–C(1)	1.94(2)	N(1)–C(1)	1.17(2)
P(2)–C(3)	1.77(2)		
C(2)–C(3)	1.27(2)		
Bond Angles			
Pt(1)–Pt(2)–Pt(1)*	163.71(6)	Pt(2)–Pt(1)–P(1)	86.6(1)
Pt(2)–Pt(1)–P(2)	165.9(1)	Pt(2)–Pt(1)–C(1)	81.2(6)
P(1)–Pt(1)–P(2)	86.0(2)	P(1)–Pt(1)–C(1)	167.7(6)
P(2)–Pt(1)–C(1)	106.3(6)	Pt(1)–P(1)–C(2)	105.1(7)
Pt(1)–P(2)–C(3)	108.6(7)	Pt(1)–C(1)–N(1)	178(2)
C(1)–N(1)–C(11)	166(2)	P(1)–C(2)–C(3)	121(2)
P(2)–C(3)–C(2)	119(2)		

[a] Estimated standard deviations in parentheses.

consumed 1.5 F mol^{-1} and afforded yellow crystals of $[\{Pt(dtbpe)(XylNC)\}_2Pt](PF_6)_2$ (**15a**, 13%) and colorless crystals of $[PtH(dtbpe)(XylNC)](PF_6)$ (**16a**, 32%). Complexes **13–16** in the solid state were stable even under an aerobic atmosphere.

The elemental analyses indicated that complexes **13–15** are coordinatively unsaturated by the loss of two isocyanide molecules from $[\{Pt(diphos)(RNC)\}_2Pt(RNC)_2](PF_6)_2$. The IR spectra indicated the presence of terminal isocyanides ($\nu_{N\equiv C}$ 2135–2141 cm^{-1}), and the ^1H NMR spectra showed one environment for isocyanide ligands. Rapid ligand exchange between the coordinating and free isocyanides was observed at room temperature in the ^1H NMR spectrum of **13a** in the presence of XylNC. In the ^1H NMR spectrum of **15a**, two doublets for the ^{t}Bu groups of dtbpe were observed at δ 1.36 and 1.44 with $^3J_{PH}$ = 14 Hz, suggesting the presence of two chemically distinct

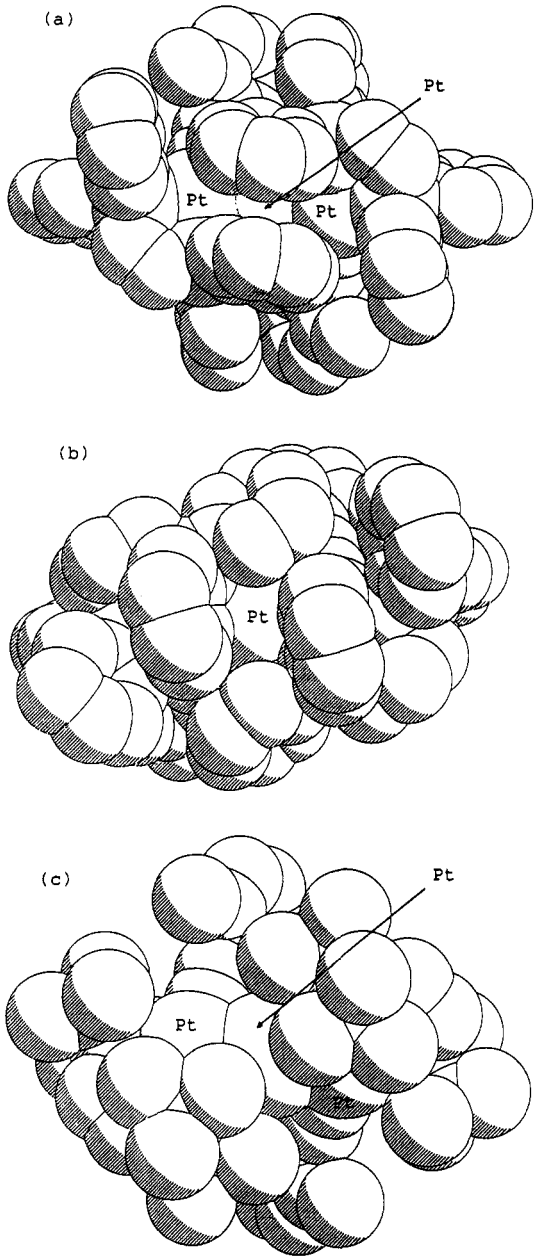

Figure 8. Space-filling drawings of the complex cations of (a) $[\{Pt(dppen)(XylNC)\}_2Pt]^{2+}$ (**13a**), (b) $[\{Pt(dppp)(XylNC)\}_2Pt]^{2+}$ (**14a**), and (c) $[\{Pt(dtbpe)(XylNC)\}_2Pt]^{2+}$ (**15a**), by using the van der Waals radii, viewed along the C_2 axis.

phosphorus atoms. The $^{31}P\{^1H\}$ NMR spectrum of **13a** showed two sets of complex resonances centered at δ 62.5 and 92.6, which were consistent with a combination of six isotopomers described for **11a** (Figure 3b). The lower field set was assigned to the P atoms lying *trans* to the Pt–Pt bonds and the higher field signal to those lying *cis* to the Pt–Pt bonds, on the basis of the coupling constants (Table 3). The satellites arising from the P_2Pt–^{195}Pt–Pt_2 isotomoper (AA'BB'X) were broad, and their intensities were weaker than expected from the natural abundance. The most prominent feature is the extremely large values of two- and three-bond couplings, $^2J_{PPt}$ = 1632 Hz, $^3J_{PPt}$ = 286 Hz, and $^2J_{P'Pt}$ = 218 Hz, and of *trans* P–P coupling, $^4J_{PP}$ = 100 Hz, in comparison with those of **11a**. A long-range coupling of $^4J_{PP'}$ = 5 Hz was also observed in addition to the *cis* coupling of $^2J_{PP'}$ = 10 Hz. The $^{31}P\{^1H\}$ NMR spectrum of **15a** exhibited two similar sets of resonances centered at δ 102.0 and 126.7, considerably shifted to the lower field compared with those in **13a**. The large couplings of $^2J_{PPt}$ = 1505 Hz, $^3J_{PPt}$ = 273 Hz, $^4J_{PP}$ = 89 Hz, and $^2J_{P'Pt}$ = 117 Hz were also derived from the spectrum, while the long-range *cis* coupling of $^4J_{PP'}$ was not resolved. The electronic absorption spectra of unsaturated complexes **13–15** showed similar patterns to those of saturated complexes **10–12** (Figure 2b), indicating the linear triplatinum structure with diphosphines chelating to the outer platinum atoms. However, the lowest energy absorption band in **13–15** was blue-shifted by 30–80 nm in comparison with that in **10–12**. The blue shift was reflected in the Pt–Pt bond lengths (*vide infra*).

The Fourier transforms of EXAFS oscillations of **13a** and **14a** are shown in Figure 5; each consists of three peaks in the range 1.1–2.7 Å (before phase-shift correction), corresponding to back-scattering contributions of the terminal carbon atom of isocyanide, the phosphorus atoms of diphosphine, and the neighboring platinum atom, respectively, which were similar to that of **10a** and **19**. These peaks were back Fourier transformed by the use of a proper window and were subjected to curve-fitting analysis using empirical parameters derived from **8b** (Table 5). The Pt–Pt bond lengths of **13a** and **15a** were determined to be 2.633 and 2.648 Å and were slightly shorter than those of the corresponding coordinatively saturated trimers, **11a** (2.650 Å (EXAFS) and 2.655 Å (crystallography)) and **12a** (2.664 Å (EXAFS)). The shortening of the Pt–Pt bonds is consistent with the electronic absorption and $^{31}P\{^1H\}$ NMR spectra (blue shift of the band maxima and the large coupling constants of $^2J_{PPt}$).

Some attempts to prepare the coordinatively unsaturated triplatinum clusters by chemical methods were not successful. As mentioned above, the treatment of **6a** with $Pt^0_3(XylNC)_6$ gave the coordinatively saturated trimer **11a**, and some attempts to convert **11a** to **13a** by thermal and electrochemical reactions also led to recovery of the starting material. These clearly indicate the importance of electrochemical processes for the formation of the coordinatively unsaturated triplatinum clusters. Although there is no direct evidence, one could speculate that an extremely active zerovalent platinum atom without any ligands was generated on the surface of the mercury electrode and was trapped by $[Pt_2(diphos)_2(RNC)_2]^{2+}$. Further, it is notable that the treatment of **13–15** with isocyanides did not produce the corresponding coordinatively saturated trimers, as summarized below.

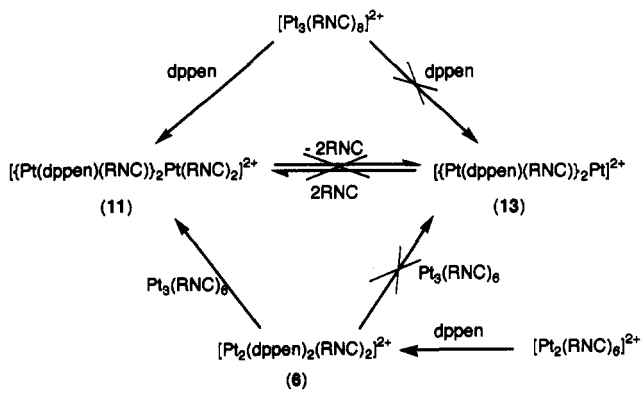

The IR spectrum of **16a** showed the presence of terminal isocyanide ($\nu_{N\equiv C}$ 2166 cm^{-1}) and hydride (ν_{PtH} 2031 cm^{-1}).

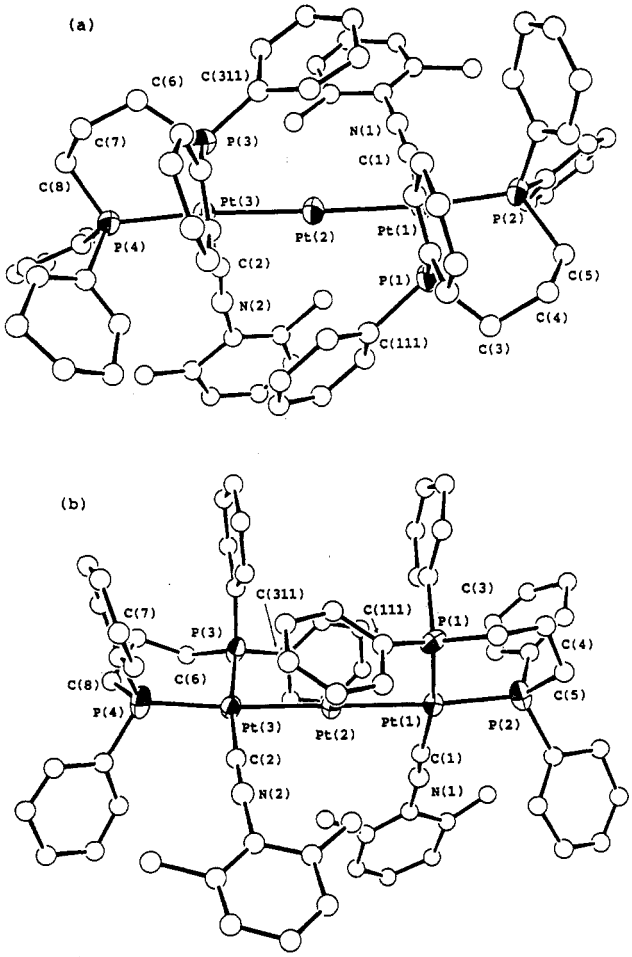

Figure 9. A perspective drawing of the complex cation of **14a**, $[\{Pt(dppp)(XylNC)\}_2Pt]^{2+}$, (a) viewed along the virtual C_2 axis and (b) vertical to the virtual C_2 axis.

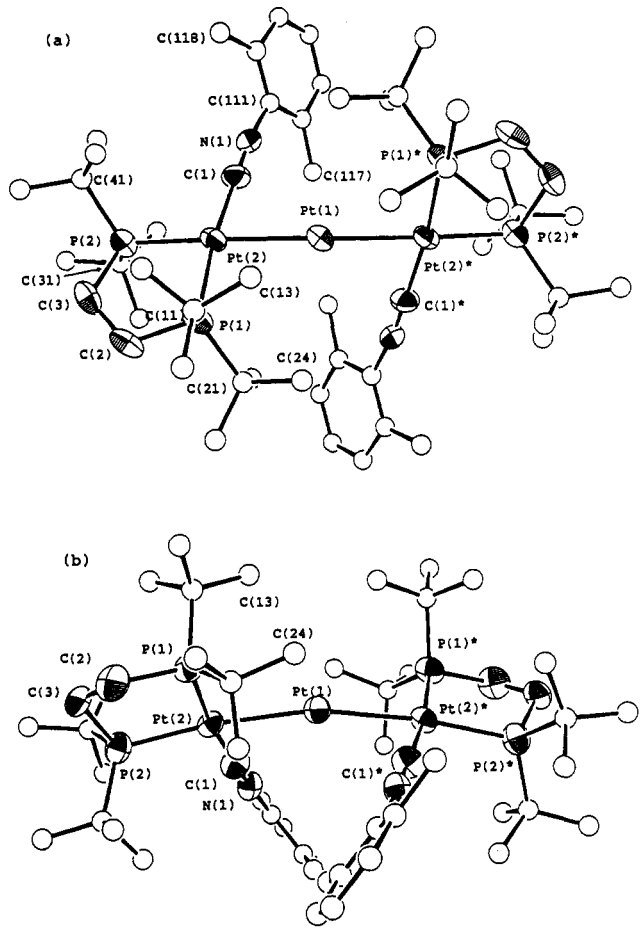

Figure 10. A perspective drawing of the complex cation of **15a**, $[\{Pt(dtbpe)(XylNC)\}_2Pt]^{2+}$, (a) viewed along the C_2 axis and (b) vertical to the C_2 axis.

The ^1H NMR spectrum exhibited the hydride resonance centered at δ −2.85 as a doublet of doublets with ^{195}Pt satellites (J_{HPt} = 912 Hz, $J_{HP(trans)}$ = 162 Hz, and $J_{HP(cis)}$ = 12 Hz). The molecular structure was confirmed by an X-ray crystallographic analysis (Figure 6). The central platinum atom is coordinated by a bidentate dtbpe, an isocyanide, and a hydrogen atom in a square planar array; the distances of Pt–P (2.284(2), 2.350(2) Å), Pt–C (1.947(8) Å), and Pt–H (1.78 Å) fall within the normal range. The Pt(1)–P(2) distance is elongated by 0.066 Å compared with that of Pt(1)–P(1) due to the high *trans* influence of the hydride ligand. The five-membered chelate ring comprising dtbpe adopts a *gauche* conformation (P(1)–Pt(1)–P(2) = 88.87(8)°). The yield of **16a** increased and that of **15a** decreased with increasing charge consumed, implying that the hydride complex was formed via a zerovalent species. The ^{t}Bu groups of dtbpe were assumed to be the hydrogen source in light of the experimental results as follows: (1) the electroreduction of **5a** in CD_3CN gave **16a** exclusively containing the Pt–H moiety, (2) the electroreduction of $[Pt(dtbpe)(RNC)_2](PF_6)_2$ (R = Ph, *p*-Tol) also afforded the corresponding hydride complexes, and (3) the electrolysis of $[Pt(dmpe)(XylNC)_2](PF_6)_2$ (dmpe = 1,2-bis(dimethylphosphino)ethane) gave no hydride complex.

When dppb was used as a source of diphosphine ligands, dark green crystals of a Hg–Pt mixed metal cluster, $[HgPt_6(dppb)_2(RNC)_8]\cdot C_6H_6$ (**17a**, R = Xyl, 11%; **17b**, R = Mes, 41%), were obtained by the electroreduction of **4** at −1.8 V (consumed 2.0 F mol^{-1}).[38,39] In this case, no linear triplatinum cluster was obtained. Mixed metal cluster **17** could also be prepared by 1% Na/Hg reduction of $PtCl_2$(COD) in the presence of dppb and isocyanide, and it has a cage-type structure where a mercury atom was incorporated into a trigonal-antiprismatic platinum core, two Pt_3 triangles being bridged by two dppb ligands.[39,40] The length of the methylene chain of the diphosphines dramatically influenced the structure of clusters produced by electrochemical reactions.

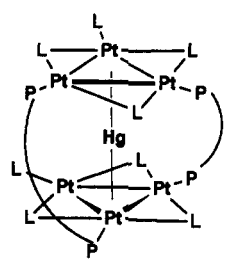

(**17**) L = RNC, P⌒P = dppb

Crystal Structure of $[\{Pt(diphos)(XylNC)\}_2Pt](PF_6)_2$ (diphos = dppen (13a), dppp (14a), and dtbpe (15a)). A single crystal of **13a** with solvated acetonitriles was obtained by recrystallization from acetonitrile/diethyl ether and was used in an X-ray crystallographic analysis. The unit cell contains two discrete complex cations, four hexafluorophosphate anions, and two loosely entrapped acetonitrile molecules separated by normal distances. A

Table 8. Selected Bond Distances (Å) and Angles (deg) of 14a[a]

Bond Distances			
Pt(1)–Pt(2)	2.645(2)	Pt(2)–Pt(3)	2.635(2)
Pt(1)–P(1)	2.28(1)	Pt(1)–P(2)	2.31(1)
Pt(1)–C(1)	1.91(4)	Pt(3)–P(3)	2.29(1)
Pt(3)–P(4)	2.31(1)	Pt(3)–C(2)	1.89(3)
P(1)–C(3)	1.79(4)	P(2)–C(5)	1.82(3)
P(3)–C(6)	1.83(4)	P(4)–C(8)	1.89(4)
N(1)–C(1)	1.18(4)	N(2)–C(2)	1.16(4)
C(3)–C(4)	1.46(4)	C(4)–C(5)	1.47(4)
C(6)–C(7)	1.55(5)	C(7)–C(8)	1.53(5)
Bond Angles			
Pt(1)–Pt(2)–Pt(3)	178.41(9)	Pt(2)–Pt(2)–Pt(1)–P(2)	173.1(3)
Pt(2)–Pt(1)–P(1)	87.6(2)	P(1)–Pt(1)–P(2)	92.9(4)
Pt(2)–Pt(1)–C(1)	82(1)	P(2)–Pt(1)–C(1)	98(1)
P(1)–Pt(1)–C(1)	169(1)	Pt(2)–Pt(3)–P(4)	172.8(3)
Pt(2)–Pt(3)–P(3)	87.8(2)	P(3)–Pt(3)–P(4)	93.5(4)
Pt(2)–Pt(3)–C(2)	84(1)	P(4)–Pt(3)–C(2)	94(1)
P(3)–Pt(3)–C(2)	172(1)	Pt(1)–P(2)–C(5)	117(1)
Pt(1)–P(1)–C(3)	114(1)	Pt(3)–P(4)–C(8)	116(1)
Pt(3)–P(3)–C(6)	115(1)	Pt(3)–C(2)–N(2)	177(3)
Pt(1)–C(1)–N(1)	169(3)	C(2)–N(2)–C(21)	172(4)
C(1)–N(1)–C(11)	168(4)	P(2)–C(5)–C(4)	118(2)
P(1)–C(3)–C(4)	118(3)	P(4)–C(8)–C(7)	118(3)
P(3)–C(6)–C(7)	109(3)	C(6)–C(7)–C(8)	113(3)
C(3)–C(4)–C(5)	115(3)		

[a] Estimated standard deviations in parentheses.

Table 9. Selected Bond Distances (Å) and Angles (deg) of 15a[a]

Bond Distances			
Pt(1)–Pt(2)	2.6409(8)	Pt(2)–P(2)	2.337(4)
Pt(2)–P(1)	2.308(4)	P(1)–C(2)	1.94(1)
Pt(2)–C(1)	1.94(1)	N(1)–C(1)	1.17(1)
P(2)–C(3)	1.87(1)		
C(2)–C(3)	1.50(2)		
Bond Angles			
Pt(2)–Pt(1)–Pt(2)*	167.24(4)	Pt(1)–Pt(2)–P(1)	94.0(1)
Pt(1)–Pt(2)–P(2)	173.2(1)	Pt(1)–Pt(2)–C(1)	78.7(4)
P(1)–Pt(2)–P(2)	88.6(1)	P(1)–Pt(2)–C(1)	172.6(4)
P(2)–Pt(2)–C(1)	98.8(4)	Pt(2)–P(1)–C(2)	105.4(5)
Pt(2)–P(2)–C(3)	105.8(5)	Pt(2)–C(1)–N(1)	179(1)
C(1)–N(1)–C(11)	171(1)	P(1)–C(2)–C(3)	117(1)
P(2)–C(3)–C(2)	112.4(9)		

[a] Estimated standard deviations in parentheses.

perspective drawing of the complex cation along with the atomic numbering scheme is given in Figure 7, and selected bond distances and angles are listed in Table 7. The complex cation consists of a linear aggregation of three platinum atoms with the central platinum atom located on a crystallographic C_2 symmetry axis. The most surprising feature is that the central platinum atom (Pt(2)) is coordinatively unsaturated without any organic ligands, being bound only to two neighboring platinum atoms. The closest neighbor of the Pt(2) atom (other than the platinum atoms) is the terminal carbon of isocyanide on the adjacent platinum with a Pt(2)···C(1) distance of 3.01(2) Å, which is clearly out of the bonding range and indicates a very weak interaction, if one exists at all. As far as we know, structurally characterized metal clusters that contain a ligand-free, coordinatively unsaturated metal center are extremely rare.[41] A detailed examination

(38) The electroreduction of **4** at a mercury pool electrode at −1.8 V vs Cp_2Fe/Cp_2Fe^+ (consumed 2 F mol^{-1}) produced a green suspension in acetonitrile, which was collected, dried in vacuo, and extracted with benzene. Crystallization from benzene/hexane gave dark green microcrystals of **17**. The analytical and spectral data were described in ref 39, and details will be reported elsewhere.

(39) Tanase, T.; Horiuchi, T.; Yamamoto, Y.; Kobayashi, K. *J. Organomet. Chem.* **1992**, *440*, 1.

Table 10. Structural Parameters of Clusters 13a, 14a, and 15a

	13a	14a	15a
Pt–Pt, Å	2.615(1)	2.640[a]	2.6409(8)
Pt–P_{ax}, Å	2.297(5)	2.31[a]	2.337(4)
Pt–P_{eq}, Å	2.260(5)	2.29[a]	2.308(4)
Pt–C, Å	1.94(2)	1.90[a]	1.94(1)
N–C, Å	1.17(2)	1.17[a]	1.17(1)
Pt–Pt–Pt, deg	163.71(6)	178.41(9)	167.24(4)
Pt–Pt–P_{ax}, deg	165.9(1)	173.0[a]	173.2(1)
Pt–Pt–P_{eq}, deg	86.6(1)	87.7[a]	94.0(1)
Pt–Pt–C, deg	81.2(6)	83[a]	78.7(4)
P–Pt–P, deg	86.0(2)	93.2[a]	88.6(1)
Pt–C–N, deg	178(2)	173[a]	179(1)
C–N–C, deg	166(2)	170[a]	171(1)
$Pt_3\cdot\cdot\cdot C_{RNC}$, Å[b]	3.01(2)	3.04(4), 3.09(2)	2.95(1)
$Pt_c\cdot\cdot\cdot C_{PR}$, Å[c]	3.37(2) (C(126))	3.42(3) (C(111)) 3.42(4) (C(311))	3.56(1) (C(24))
θ, deg[d]	59	85	73

[a] Average value. [b] The interatomic distance between the central platinum atom and the terminal carbon atom of isocyanide on the outer platinum atom. [c] The minimum interatomic distance between the central platinum atom and the carbon atoms in the substituents on the phosphorus atoms. [d] The dihedral angle between the coordination planes around the outer platinum atoms.

of the bonding system is extremely important in relation to the surface of heterogeneous catalysts. The outer platinum (Pt(1)) is coordinated by a bidentate dppen ligand, a terminal isocyanide, and the central platinum atom in a distorted square planar geometry. The twist angle between the two square planes is 59° ([Pt(1)Pt(2)P(1)P(2)C(1)] vs [Pt(1)*Pt(2)P(1)*P(2)*C(1)*]), distorted by ~30° from the perpendicular to avoid steric repulsion between the phenyl groups on the equatorial P atoms. There is no interaction (<3.3 Å) between the central platinum atom and phenyl rings on the P atoms, but the ligand-free Pt center is covered by the two axially oriented phenyl groups with respect to the chelate ring as shown in Figure 8a. The steric arrangement may be one of the important factors for the successful isolation of the naked cluster. The triplatinum core is slightly deformed from linearity, with a Pt(1)–Pt(2)–Pt(1)* angle of 163.71(6)° (toward the upper direction in Figure 7b). The Pt(1)–Pt(2) bond length is 2.615(1) Å, which is shorter than those of the trimers **11a** (2.655(1) Å) and **19** (2.6389(7) Å). The shortening of the metal–metal bond is presumably attributed to the absence of organic ligands on the central platinum atom. The two axial P atoms are collinear with the Pt–Pt bond, with a Pt(2)–Pt(1)–P(2) angle of 165.9(1)°. The P(2)–Pt(1) bond length (2.297(2) Å) is longer by 0.037 Å than the P(1)–Pt(1) bond distance (2.260(2) Å), indicating a *trans* effect of the Pt–Pt bond. The five-membered chelate ring comprising dppen adopts an envelope form with the platinum atom at the flap (the torsion angle of P(1)–C(2)–C(3)–P(2) is 0(3)°). The *cis* angle of P(1)–Pt(1)–P(2) is 86.0(2)°, comparable to that found in **11a**. The inward bend of the terminal isocyanide is observed with the Pt(2)–Pt(1)–C(1) angle of 81.2(6)°, which is almost equal to that found in the diplatinum compound **8b** (average 81.5°). Generally, triplatinum complexes are known to have 42 or 44 valence electrons,[4,42,43] but the present coordinatively unsaturated

(40) (a) Yamamoto, Y.; Yamazaki, H. *J. Am. Chem. Soc.* **1982**, *104*, 2329. (b) Yamamoto, Y.; Yamazaki, H. *J. Chem. Soc., Dalton Trans.* **1989**, 2161.

(41) Nagle, J. K.; Balch, A. L.; Olmstead, M. M. *J. Am. Chem. Soc.* **1988**, *110*, 319.

(42) Gubin, S. *Russ. Chem. Rev.* **1985**, *54*, 529.

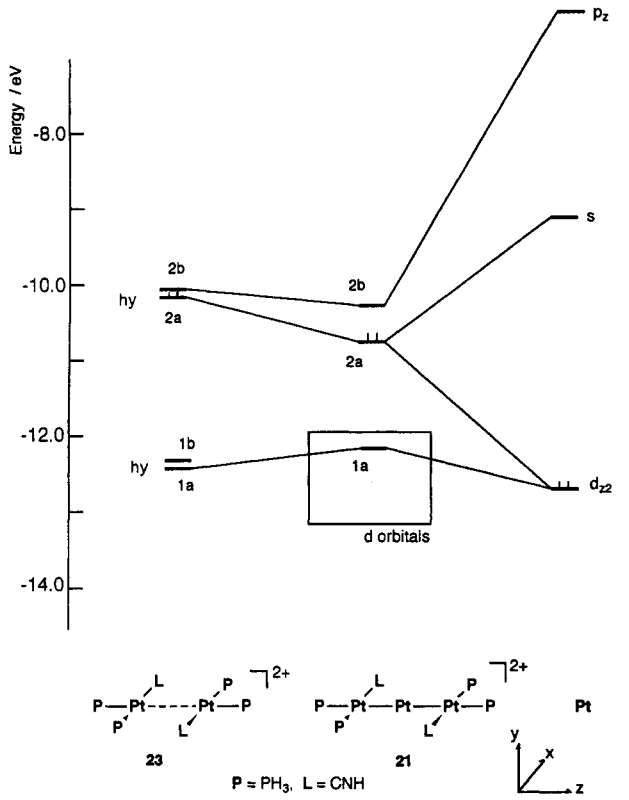

Figure 11. An interaction diagram for $[\{Pt(PH_3)_2(HNC)\}_2Pt]^{2+}$ (**21**) in terms of the fragments $[Pt(PH_3)_2(HNC)\cdots Pt(PH_3)_2(HNC)]^{2+}$ and Pt^0.

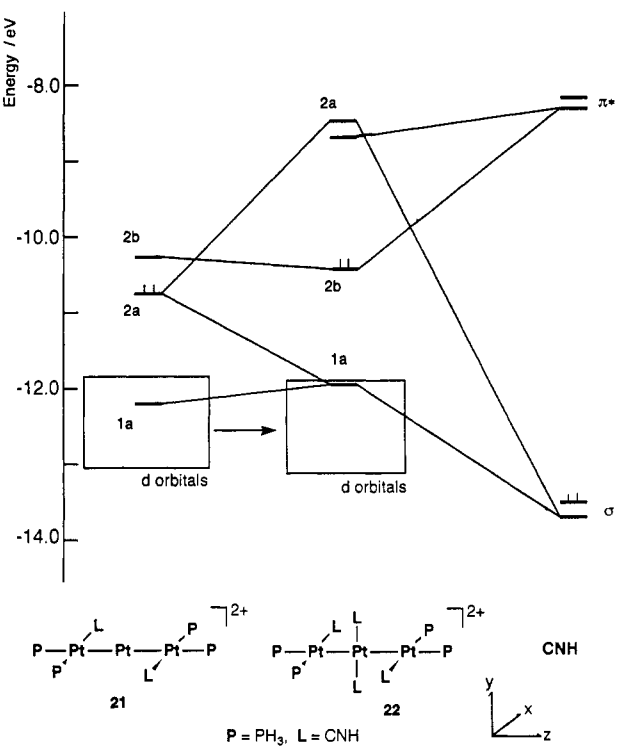

Figure 12. An interaction diagram for $[\{Pt(PH_3)_2(HNC)\}_2Pt(HNC)_2]^{2+}$ (**22**) in terms of fragments **21** and $(HNC)_2$.

complex has an unprecedented 40 valence electrons and is thus extremely electron deficient.

The crystal structures of the complex cations of **14a** and **15a** are given in Figures 9 and 10, and selected bond lengths and angles are presented in Tables 8 and 9. The cations of **14a** and **15a** are isostructural with that of **13a**. The structural parameters are summarized in Table 10. The cation of **14a** has a pseudo C_2 symmetry axis on the Pt(2) atoms, and that of **15a** has a crystallographically imposed C_2 symmetry. The triplatinum core of **14a** is almost linear (Pt–Pt–Pt = 178.41(9)°), and that of **15a** is bent toward the opposite direction of that in **13a** (Pt–Pt–Pt = 167.24(4)°) due to the steric bulk of dtbpe ligands (Figures 9b and 10b). These findings suggested that the linear triplatinum core is likely deformed depending on the steric bulkiness of the diphosphine ligand. The Pt–Pt bond distances are 2.640 Å (mean value) (**14a**) and 2.6409(8) Å (**15a**), which are longer than that found in **13a**, but still shorter than those of the coordinatively saturated dimer **8b** (2.653(2) Å) and trimer **11a** (2.655(1) Å). The two square planes around the outer platinum atoms are nearly perpendicular, with dihedral angles of 85° (**14a**) and 73° (**15a**).

In compound **14a**, the six-membered chelate ring comprising dppp adopts a stable chair form with an average bit angle of 93.2°. The orientation of the phenyl rings is considerably different from that found in the dppen compound **13a**, owing to the difference of chelate ring conformations. The equatorially oriented phenyl groups on the P(1) and P(3) atoms with respect to the chelate rings hang over the central platinum atom, but no definite interaction (<3.3 Å) is observed (Figure 8b). The terminal isocyanides are bent toward the middle of the cluster (Pt(2)–Pt(1)–C(1) = 82(1)° and Pt(2)–Pt(3)–C(2) = 84(1)°). The interatomic distances between the terminal carbon atoms of isocyanides and the Pt(2) atom are 3.04(4) Å (Pt(2)···C(1) and 3.09(3) Å (Pt(2)···C(2)), both of which are out of bonding range.

In compound **15a**, the five-membered chelate ring takes a *gauche* conformation and the bite angle is 88.6(1)°, slightly larger than that of **13a**. The ^{t}Bu groups on the P(1) atom are occupied rather away from the central platinum atom, but their bulkiness is seemingly enough to protect the ligand-free platinum center (Figure 8c). The inward bend of the terminal isocyanides is somewhat greater (Pt(1)–Pt(2)–C(1) = 78.7(4)°) than those found in **13a** and **14a**, resulting in a relatively short interatomic distance between the Pt(1) atom and the terminal carbon atom of isocyanide (Pt(2)···C(1) = 2.95(1) Å).

Molecular Orbital Descriptions. Extended Hückel molecular orbital calculations were carried out on the model compounds $[\{Pt(PH_3)_2(HNC)\}_2Pt]^{2+}$ (**21**) and $[\{Pt(PH_3)_2(HNC)\}_2\,Pt(HNC)_2]^{2+}$ (**22**), to elucidate the electronic structure of the coordinatively unsaturated and saturated triplatinum clusters.[44]

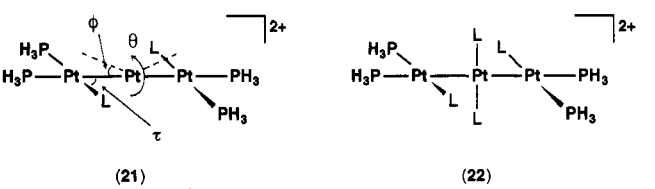

The total energies and the electronic structure of the staggered (θ = 90°) and eclipsed (θ = 0°) forms of **21** are almost identical, so we adopt the eclipsed model of **21** to

(43) (a) Mingos, D. M. P.; Evance, D. G. *J. Organomet. Chem.* **1983**, *251*, C13. (b) Mingos, D. M. P. *Acc. Chem. Res.* **1984**, *17*, 311.

(44) The phosphorus atom d orbitals were not included in the present calculations to simplify the interactions of valence orbitals, whereas the calculations in the preliminary report included them. The essential features are identical in both cases.

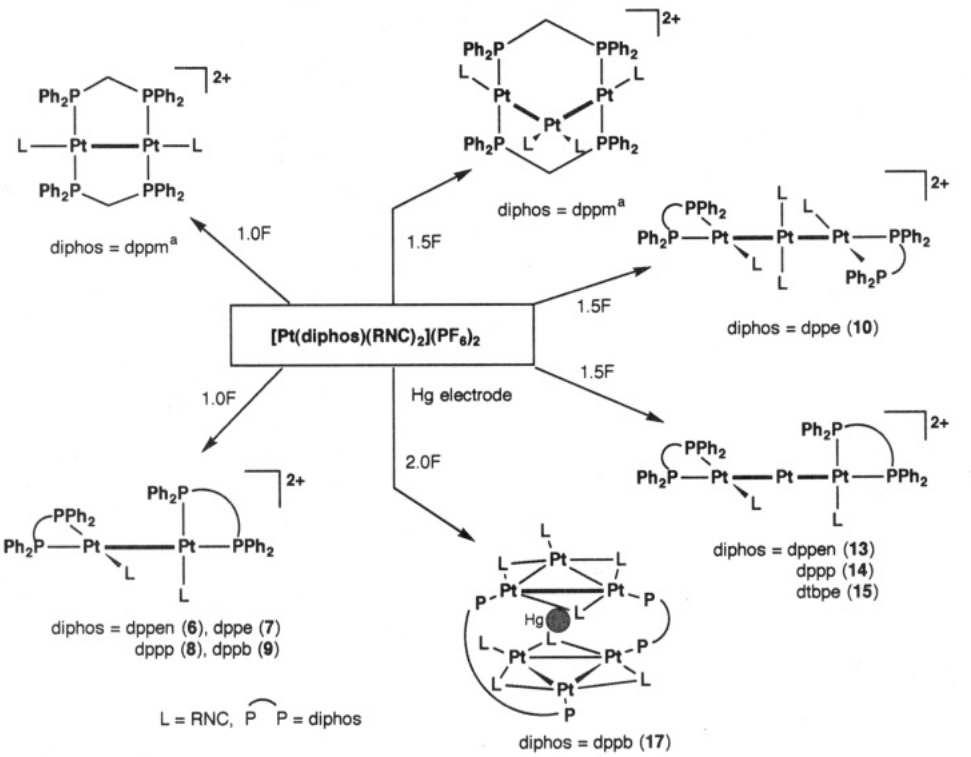

Figure 13. Electrochemical preparations of di-, tri-, and polynuclear platinum complexes containing diphosphines and isocyanides. (a) References 7 and 8.

clarify its relation to the coordinatively saturated model **22**. An interaction diagram for **21** in terms of the fragments $[Pt(PH_3)_2(HNC)\cdots Pt(PH_3)_2(HNC)]^{2+}$ (**23**) and Pt^0 is illustrated in Figure 11. The HOMO is derived from a bonding interaction between the filled d orbital (2a, a hybrid of d_{z^2} and $d_{x^2-y^2}$) of the fragment **23** and the empty s orbital of the central Pt atom, and it is destabilized by a repulsive interaction with the filled d_{z^2} orbital of the central Pt atom. This is the dominant bonding mode, and the bonding electrons are localized on the central platinum atom. Thus, the net charge is also localized on the central platinum (−0.78 on the central Pt and +0.23 on the outer Pt), suggesting that the ligand-free platinum is essentially labile. The LUMO consists of a bonding interaction between the d orbital (2b, a hybrid of d_{z^2} and $d_{x^2-y^2}$) of the fragment **23** and the empty p_z orbital of the central Pt atom. The energy gap between the HOMO and the LUMO is very small (0.48 eV). These results imply that the coordinatively unsaturated triplatinum clusters (**13**–**15**) are electronically unstable. Their apparent stabilities are therefore probably due to the steric effects of the diphosphine and isocyanide ligands, which overcome electronic instability.

With an increase of ϕ in **21**, the HOMO is stabilized by a decrease of the 2a − d_{z^2} antibonding overlap and the LUMO is destabilized by a decrease of the 2b − p_z bonding interaction, resulting in an increase of the HOMO–LUMP gap. The conformation at $\phi = 20°$ gains a stabilization energy of −0.26 eV, at which the HOMO–LUMO energy gap is expanded to 0.79 eV. The profile of the total energy as a function of the angle τ shows a minimum at $\tau = 75°$ (the stabilization energy is 0.32 eV), due to a weak interaction of the filled d orbitals of the central Pt atom with the empty π^* orbitals of HNC as reported in the coordinatively saturated di- and trinuclear platinum and palladium complexes.[36,37] The donating interaction from the HNC groups to the naked Pt center is not observed at all.

An interaction diagram for **22** in terms of the fragments **21** and $(HNC)_2$ is given in Figure 12. The filled 2a orbital of **21** interacts well with the filled σ orbitals of the $(HNC)_2$ fragment, and the HOMO of **22** consists of a bonding interaction of the empty 2b orbital of **21** with the empty π^* orbitals of $(HNC)_2$. The formation energy of **22** from the fragments **21** and $(HNC)_2$ is −3.80 eV. The HOMO–LUMO energy gap in **22** is larger (1.76 eV) than that of **21**. These bonding modes lead to a delocalization of the charge on the central platinum into the π^* orbitals of the central HNC groups, which is evident in the net charge distribution, −0.24 on the central Pt and −0.10 on the outer Pt. The difference of the charge distribution between **21** and **22** was supported by the fact that a charge separation between the inner and outer Pt atoms was observed in the XPS (ESCA) of the coordinatively unsaturated complex **14a**, but that it was not observed in that of the saturated complex **10a**.[45]

Conclusion. A variety of metal–metal bonded platinum complexes of diphosphines were prepared by electrochemical techniques controlling the potential and the charge consumed (Figure 13). The one-electron reduction of $[Pt(diphos)(RNC)_2]^{2+}$ gave the dinuclear platinum complexes, $[Pt_2(diphos)_2(RNC)_2]^{2+}$, in which the dppm acted as a bridging ligand[8] and the dppen, dppe, dppp, and dppb ligands chelated to the platinum atom. In the 1.5-electron reductions, the structures of the platinum clusters obtained were dramatically influenced by the diphosphine ligands. $[Pt(dppm)(RNC)_2]^{2+}$ was converted to the A-frame triplatinum cluster, $[Pt_3(\mu\text{-dppm})_2(RNC)_4]^{2+}$,[7,8] and $[Pt(dppe)(RNC)_2]^{2+}$ led to the linear

(45) Nakao, A. Private communication. Detailed results will be reported elsewhere.

triplatinum compound, $[\{Pt(dppe)(RNC)\}_2Pt(RNC)_2]^{2+}$. By using dppen, dppp, and dtbpe ligands, coordinatively unsaturated triplatinum clusters, $[\{Pt(diphos)(RNC)\}_2Pt]^{2+}$, were obtained. The ligand-free platinum atom is trapped in the middle of the linear aggregation and is stabilized by the steric effects of bulky diphosphines. This bonding mode could provide important information in connection with the bonding system of metal atoms near the surface of heterogeneous catalysts. When dppb was used, the Hg–Pt mixed metal cluster, $[HgPt_6(dppb)_2(RNC)_8]$, was produced instead of the triplatinum compounds. These findings strongly suggested that electrochemical techniques could be very effective in designing specific polynuclear geometrics.

We are now trying to examine the reactivity of the coordinatively unsaturated platinum complexes toward some organic reagents including carbon monoxide, carbon dioxide, and dihydrogen molecules.

Acknowledgment. This work was partially supported by a Grant-in-Aid for Scientific Research from the Ministry of Education of Japan and a grant from Futaba Denshikogyo.

Supplementary Material Available: Listings of crystallographic data, positional and anisotropic thermal parameters, atomic parameters of hydrogen atoms, and bond distances and angles for **8b**, **11a**, **13a**, **14a**, **15a**, and **16a** and results of EXAFS analyses (54 pages). Ordering information is given on any current masthead page.

OM9307500